

## On the variability of the Mediterranean Outflow Water in the North Atlantic from 1948 to 2006

Alexandra Bozec,<sup>1</sup> M. Susan Lozier,<sup>2</sup> Eric P. Chassignet,<sup>1</sup> and George R. Halliwell<sup>3</sup>

Received 1 April 2011; revised 22 June 2011; accepted 5 July 2011; published 30 September 2011.

[1] Recent work has shown that variability in the properties and/or transport of Mediterranean Seawaters spilling across the Strait of Gibraltar into the North Atlantic have had little impact on the variability of Mediterranean Outflow Water (MOW) in the that basin over the past fifty years. Here we investigate whether circulation changes are the dominant source of MOW variability in the North Atlantic between 1948 and 2006. Using a 1/3° North Atlantic configuration of the HYbrid Coordinate Ocean Model combined with the Marginal Sea Boundary Condition model, two simulations forced by either climatological or interannual atmospheric fields are performed. The interannual simulation reproduces the observed MOW variability without Mediterranean Seawater changes. Thus, we conclude that MOW variability in the last 60 years is a consequence of circulation changes in the North Atlantic. A series of simulations that separate the mechanical effect of the wind from the impact of buoyancy forcing show that MOW variability can be attributed to shifts between its dominant northward and westward pathways. The pathway shifts from predominantly northward between 1950 and 1975 to predominantly westward between 1975 and 1995 and finally back to northward after 1995. Though these pathway shifts appear to be wind-induced, the property changes are caused by the combined impact of wind and buoyancy forcing on the circulation of the North Atlantic.

**Citation:** Bozec, A., M. S. Lozier, E. P. Chassignet, and G. R. Halliwell (2011), On the variability of the Mediterranean Outflow Water in the North Atlantic from 1948 to 2006, *J. Geophys. Res.*, 116, C09033, doi:10.1029/2011JC007191.

### 1. Introduction

[2] The Mediterranean Outflow Water (MOW) is a saline and warm water mass principally occupying the intermediate depths of the eastern North Atlantic (Figure 1). This water mass is produced from the transformation of fresh and warm surface Atlantic waters into dense and salty Mediterranean water. Entering the marginal sea by the Strait of Gibraltar, Atlantic water is gradually modified during its eastward progression in the Mediterranean Sea through air-sea interactions and mixing processes. These modifications lead to the formation of salty and relatively cold intermediate and deep-water masses (see review by *Pinardi and Masetti* [2000]). A portion of these dense water masses then flows back toward the Strait of Gibraltar, reaching it after ~7 to ~70 years [*Artale et al.*, 2006]. This Mediterranean Sea Water (MSW) then cascades along the slope in the Gulf of Cadiz and mixes with the ambient North Atlantic Central Water (NACW) to form MOW. Reaching a buoyant depth around 1100 m, MOW

spreads into the North Atlantic: westward to the central Atlantic and northward following the coasts of Portugal and Spain [*Lozier et al.*, 1995]. The signature of MOW salinity can be observed as far west as Bermuda and as far north as the Rockall Trough (Figure 1). This warm and salty water mass makes an important contributor to the heat and salt content of the North Atlantic [*Zenk*, 1975; *Reid*, 1979] and has been cited as a possible contribution to the preconditioning of deep water mass formation in key areas of the global overturning circulation such as the Labrador and Nordic seas [*Reid*, 1979].

[3] Investigating the evolution of MOW properties between 1955 and 1993, *Potter and Lozier* [2004, hereinafter PL04] calculated temperature and salinity trends in a region west of the Gulf of Cadiz defined as the MOW reservoir [10°W, 20°W, 30°N, 40°N]. During this time period, PL04 found a positive temperature trend ( $0.101 \pm 0.024^\circ\text{C}/\text{decade}$ ) that far exceeds the average North Atlantic temperature trend [*Levitus et al.*, 2000] and a positive salinity trend of  $0.028 \pm 0.0067$  psu/decade. A more recent study by *Leadbetter et al.* [2007] compared the MOW properties from WOCE transects repeated along 36°N in 1959, 1981, and 2005. Their findings are consistent with those of PL04 in that they observe a warming and salinification between 1959 and 1981. However, they also found a cooling and freshening between 1981 and 2005, raising the question as to what mechanism is responsible for these property shifts in the MOW reservoir.

<sup>1</sup>Center for Ocean and Atmospheric Predictions Studies, Florida State University, Tallahassee, Florida, USA.

<sup>2</sup>Earth and Ocean Sciences, Nicholas School of the Environment, Duke University, Durham, North Carolina, USA.

<sup>3</sup>Atlantic Oceanographic and Meteorological Laboratory, NOAA, Miami, Florida, USA.

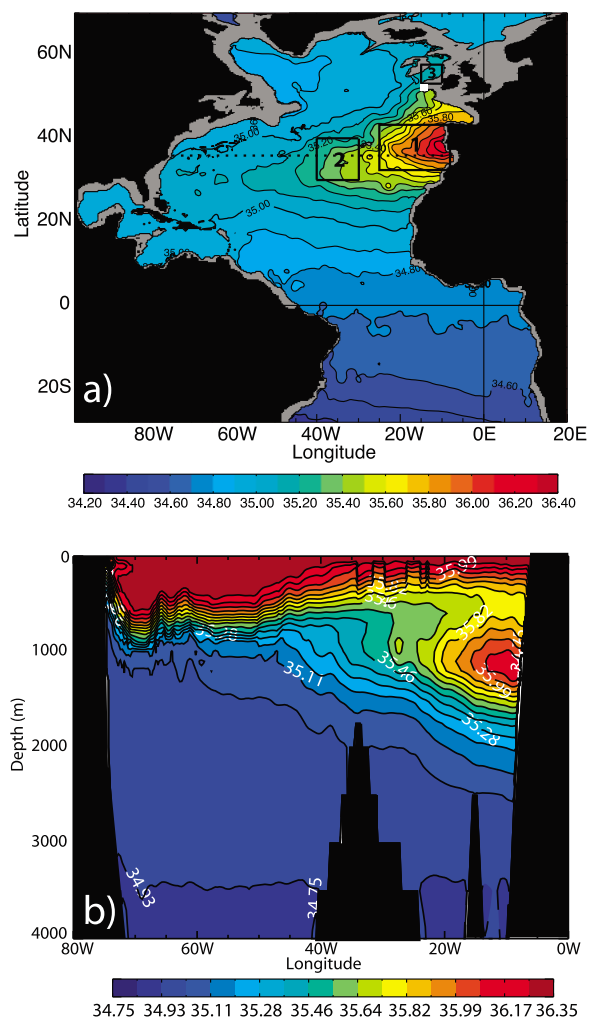


**Figure 1.** (a) Salinity at 1100 m from GDEM3 climatology on the HYCOM 1/3° Atlantic domain. Gray areas show the 1100 m isobaths. The analysis of the MOW variability is done over the reservoir and its western and northern pathways: the MOW reservoir [10°W, 25°W, 32°N, 42°N] (box 1), the central Atlantic [30°W, 40°W, 30°N, 40°N] (box 2) for the western pathway, and the Rockall Trough [11.5°W, 15°W, 52.5°N, 57.5°N] (box 3) for the northern pathway. The white square shows the location of Porcupine Bank. (b) Vertical sections of salinity at 36°N.

[4] There are three possible sources for the variability of MOW properties in the reservoir: (1) a change in MSW properties, (2) a change in NACW properties, or (3) a change in the circulation of the North Atlantic that would alter the MOW water mass distribution. *Lozier and Sindlinger* [2009] showed that the first two possibilities, namely MSW and NACW variability, are too weak to explain the observed variability of the MOW. The main goal of this study is to investigate the third possible source. In the first part of this study, we test the viability of the third hypothesis by setting up two 59-year simulations of a 1/3° North Atlantic configuration of the Hybrid Coordinate Ocean Model (HYCOM): one with climatological atmospheric forcing and one with interannual atmospheric forcing from 1948 to 2006. Since the

model resolution is too coarse to resolve the physical processes of the overflow in the Gulf of Cadiz, the model was combined with the Marginal Sea Boundary Condition box model (MSBC) [*Price and Yang*, 1998]. In the second part of this study, we investigate how interannual North Atlantic atmospheric forcing affects the MOW property variability. Three simulations are performed to separate the mechanical effect of the wind stress from the impact of buoyancy forcing on the property and flow fields of the Atlantic Ocean: (1) a simulation forced with climatological wind stress and buoyancy forcing, (2) a simulation forced with interannual wind stress and climatological buoyancy forcing, and (3) a simulation forced with interannual wind stress and buoyancy forcing. The evolution of MOW properties and the transport budgets of the reservoir for each simulation are compared to identify changes in the circulation and properties in the MOW. The variability of the water masses present in the North Atlantic is also examined to investigate how the different components of the atmospheric forcing affect water mass pathways in the North Atlantic. Taking into account the mechanism(s) involved and its (their) effect(s) on MOW pathways, the variability and extent of MOW pathways are discussed with an emphasis on MOW variability in the Rockall Trough region, which is a potential access point for MOW to the Nordic seas.

[5] The paper is organized as follows: background on the distribution of MOW is given in section 2 and the ocean model and experimental setup are presented in section 3. Results are discussed in sections 4 through 6, with the main conclusions presented in section 7.

## 2. Background on the Distribution of MOW in the North Atlantic

[6] Previous work on the distribution of MOW in the North Atlantic has identified two main advective pathways or branches of MOW: one westward and one northward. *Reid* [1994] describes the westward branch of MOW as extending beyond 35°W, however, *Iorga and Lozier* [1999a, 1999b], using 80 years of hydrographic data and a geostrophic diagnostic model, found that the westward branch of MOW mainly recirculates between 10°W and 20°W; no clear advective flow beyond 20°W was identified. This latter result is consistent with the findings of *Mazé et al.* [1997], who argue that the incursion of saline water into the North Atlantic interior is made only through the propagation of Meddies and not from a direct advection of MOW.

[7] The northern branch of MOW follows the coasts of Portugal and Spain, enters the Bay of Biscay, and continues northward toward the Rockall Trough [*Reid*, 1979, 1994; *Bower et al.*, 2002]. Several studies [*Reid*, 1979, 1994; *Iorga and Lozier*, 1999a, 1999b] that have combined hydrographic data and geostrophic models have conjectured a flow of MOW into the Rockall Trough, with some studies suggesting that this flow eventually reaches the Nordic seas [*Reid*, 1994]. Other studies present results from models [*New et al.*, 2001] or from observations [*McCartney and Mauritzen*, 2001] showing that MOW, blocked by the subpolar front, does not reach beyond Porcupine Bank (Figure 1, white square). In a more recent study, *Lozier and Stewart* [2008] tried to reconcile these two points of view (i.e., whether or not the MOW is present in the Rockall Trough) by showing that the incur-

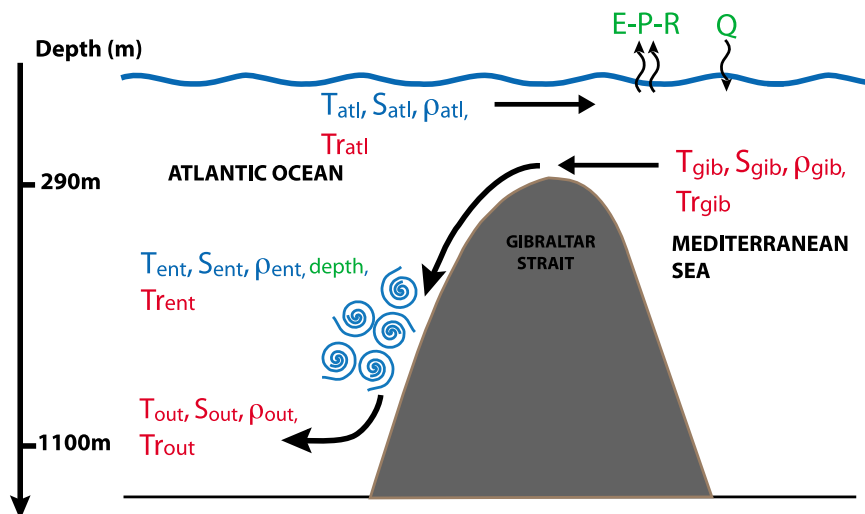


**Figure 2.** Schematic of the exchange at the Strait of Gibraltar.  $S_{atl}$  corresponds to Atlantic waters,  $S_{gib}$  corresponds to Mediterranean Sea Water at Gibraltar (source water),  $S_{ent}$  corresponds to NACW entrained water, and finally,  $S_{out}$  corresponds to outflow water. Variables in green are prescribed, variables in blue are given by HYCOM, and variables in red are calculated by the MSBC model.

sion of MOW in the Rockall Trough is significantly (anti) correlated with (eastward) westward shifts of the subpolar front between 1950 and 2000. Their results are consistent with *Holliday* [2003] and *Holliday et al.* [2008], who observe a large increase of the salinity anomaly in the upper 900 m (expected depth of the MOW at this latitude) of the Rockall Trough and the Nordic seas after 1996. These authors attribute this salinity increase to a sudden westward shift of the subpolar front that allows more water from the eastern Atlantic basin (warmer and saltier) and less water from the western Atlantic basin (cooler and fresher) to enter the Rockall Trough. In this study, we focus on the relative strengths of the western and northern branches under differing forcing conditions and investigate the resultant impact on MOW property variability.

### 3. The 1/3° North Atlantic HYCOM Configuration

#### 3.1. Description of the Model Configuration

[8] HYCOM [Bleck, 2002; Chassignet et al., 2003; Halliwell, 2004], configured for the North Atlantic is used for this study. The 1/3° resolution model domain extends from 90°W to 30°E and from 20°S to 70°N (Figure 1) and does not include the Mediterranean Sea. The bottom topography is derived from DBDB5 [National Geophysical Data Center, 1985]. The vertical discretization in HYCOM combines pressure coordinates at the surface, isopycnic coordinates in the stratified open ocean, and sigma coordinates over shallow coastal regions. Twenty-eight hybrid layers whose  $\sigma_2$  target densities range from 23.50 to 37.48 kg/m<sup>3</sup> are used. The initial conditions in temperature and salinity are given by the General Digital Environmental Model (GDEM3) [Teague et al., 1990]. Relaxation to climatology is applied at the northern and southern boundaries in 10° buffer zones. Vertical mixing is provided by the KPP model [Large et al., 1994].

[9] The climatological atmospheric forcing is derived from the 1979–1993 ECMWF climatology (ERA15). To account for synoptic atmospheric variability, 6-hourly wind stress anomalies corresponding to a neutral El Niño period (September 1984 to September 1985, identified using the Southern Oscillation Index) are added to the monthly wind stresses; wind speed is obtained from the 6-hourly wind stresses. Heat and freshwater fluxes are calculated using bulk formulae during model simulations. The heat flux is derived from surface radiation, air temperature, specific humidity, wind speed, and model sea surface temperature (SST). The freshwater flux consists of an E-P budget plus a relaxation to observed climatological surface salinity with a 30-day time scale. Evaporation is calculated from bulk formulae using wind speed, specific humidity, and model SST. Precipitation is given by COADS.

[10] The interannual atmospheric forcing covers a period of 59 years from 1948 to 2006 and is derived from the NCEP/NCAR reanalysis. To be consistent with the climatological forcing, we keep the ERA15 mean and add the 6-hourly NCEP anomalies to produce the atmospheric forcing. No interannual variability in precipitation is prescribed.

#### 3.2. Description of the MSBC

[11] Characteristics of the MSBC model are illustrated schematically in Figure 2. Using information about North Atlantic surface waters in the Gulf of Cadiz ( $T_{atl}$ ,  $S_{atl}$ ,  $\rho_{atl}$ ) and the heat and evaporation budget ( $Q$ ,  $E-P-R$ ) over the Mediterranean Sea, the model first computes the properties ( $T_{gib}$ ,  $S_{gib}$ ,  $\rho_{gib}$ ) and transport ( $Tr_{gib}$ ) of the MSW at Gibraltar. The model then calculates properties ( $T_{out}$ ,  $S_{out}$ ,  $\rho_{out}$ ) and transport ( $Tr_{out}$ ) of the final overflow water by entraining the NACW properties ( $T_{ent}$ ,  $S_{ent}$ ,  $\rho_{ent}$ ) into the MSW. The reader is referred to *Price and Baringer* [1994] and *Price and Yang* [1998] for a more detailed explanation of the model. Although the MSBC is a relatively simple model of the out-

**Table 1.** Description of the Simulations of This Study

	CLIM1	INTER1	CLIM2	WIND	INTER2
Length of simulation	89 years	59 years	59 years	59 years	59 years
MOW $T$ , $S$ , $T_r$	Given by MSBC	Given by MSBC	Prescribed at 11°C, 36.2 psu and 4 Sv	Prescribed at 11°C, 36.2 psu and 4 Sv	Prescribed at 11°C, 36.2 psu and 4 Sv
Atmospheric forcing	Climatology 1979–1993 ECMWF for flux and wind	Interannual NCEP/NCAR 1948–2006 for flux and wind	Climatology 1979–1993 ECMWF for flux and wind	Climatology 1979–1993 ECMWF for flux and interannual NCEP/NCAR 1948–2006 for wind	Interannual NCEP/NCAR 1948–2006 for flux and wind

flow process, results have been shown to be as accurate as numerical model results using the parameterization of *Xu et al.* [2007] for the Mediterranean outflow region.

### 3.3. Implementation and Parameters of the MSBC in HYCOM

[12] Since the model resolution ( $1/3^\circ$ ) is not sufficient to resolve the physical processes of the overflow in the Gulf of Cadiz, we implement the MSBC model in HYCOM. The Gulf of Cadiz becomes a boundary zone (between  $\sim 6^\circ\text{W}$  to  $\sim 8^\circ\text{W}$ ) where the MSBC model determines the water properties, depth range, and transport of the overflow water entering the Atlantic basin. Inputs to the MSBC model are either specified or provided by the model at grid points just west of the Gulf of Cadiz boundary zone.

[13] Specified inputs are the depth where the entrainment occurs, the mass ( $E-P-R$ ) and net surface heat ( $Q$ ) fluxes averaged over the Mediterranean Sea. *Price and Baringer* [1994] prescribe values of 0.7 m/y and 0 W/m<sup>2</sup> for the freshwater and heat flux, respectively. In the observations, the freshwater flux of the Mediterranean Sea has been estimated between 0.52 m/y and 0.96 m/y [*Garrett, 1996; Béthoux and Gentili, 1999*], and the average net heat flux has been estimated at  $-7\text{ W/m}^2$  with variations of  $\pm 15\text{ W/m}^2$  between 1945 and 1990 [*Garrett et al., 1993*]. The values of 0.55 m/y and  $-13\text{ W/m}^2$  were found to provide MSW properties close to the observations for this configuration of HYCOM. In the Gulf of Cadiz, most of the entrainment occurs in the first 50 km outside the Strait of Gibraltar between 350 m and 600 m [*Price and Baringer, 1994*]. Since the Gulf of Cadiz boundary zone expands to  $8^\circ\text{W}$ , where the entrainment occurs in the lower depth range of the observations, the depth of the entrainment was set to 625 m.

[14] The inputs provided by HYCOM (highlighted in blue in Figure 2) to the MSBC model are the Atlantic inflow temperature and salinity ( $T_{atl}$ ,  $S_{atl}$ ) averaged over the upper 140 m just west of the Gulf of Cadiz boundary zone, and the temperature and salinity of the entrained NACW ( $T_{ent}$ ,  $S_{ent}$ ) at the prescribed depth of 625 m. The MSBC outputs (highlighted in red in Figure 2) include four transports:  $Tr_{atl}$ ,  $Tr_{gib}$ ,  $Tr_{ent}$ , and  $Tr_{out}$ , with the first two being equal but of opposite sign. The outputs also include the temperature and salinity of the Gibraltar outflow ( $T_{gib}$ ,  $S_{gib}$ ) and the MOW ( $T_{out}$ ,  $S_{out}$ ). The corresponding densities are calculated using the model equation of state.

[15] Implementation of the MSBC in HYCOM requires that MOW, which has a temperature and salinity calculated by the MSBC, be accepted by interior isopycnic layers under the condition that the target isopycnic density in each

accepting layer is preserved. Technical details of the MSBC implementation are described fully in the Appendix.

## 4. Examination of Circulation Changes as a Source of MOW Variability

[16] To test the viability of the hypothesis that changes in MOW result from circulation changes in the North Atlantic, we use the  $1/3^\circ$  Atlantic Ocean configuration of the HYbrid Coordinate Ocean Model (HYCOM) described in section 3 and perform two simulations, CLIM1 and INTER1, forced by climatological atmospheric fields (steady state simulation) and interannual atmospheric fields (realistic simulation), respectively. CLIM1 is integrated for a total of 89 years, while INTER1 is integrated for 59 years starting from year 30 of CLIM1 (spin-up period) (Table 1). The realistic simulation covers the period 1948–2006. In these particular simulations the MOW temperature, salinity and transport are given by the MSBC. Also, for the purpose of comparing the results with observed trends, the main focus is on the period 1955–1993.

### 4.1. Main Features of the MOW as Modeled by HYCOM

[17] Before comparing MOW modeled variability with MOW observed variability, we assess the suitability of the model to reproduce the observed mean MOW properties and circulation pathways. The MOW tongue in CLIM1 and INTER1 (Figure 3) is similar to the MOW tongue in the GDEM3 climatology (Figures 1a and 1b) in terms of overall shape, extent and strength. The modeled MOW is contained within layers  $\sigma_2 = 36.38\text{ kg/m}^3$  and  $\sigma_2 = 36.52\text{ kg/m}^3$  (layers 14 and 15 of the model), isopycnic surfaces that are neutrally buoyant around 1100 m in the vicinity of the Gulf of Cadiz. The salty water in the model simulations ( $S > 35.40$  psu) spreads westward to  $40^\circ\text{W}$  and northward to  $50^\circ\text{N}$ , as in GDEM3. The vertical structure of MOW from the model simulations is also very similar to GDEM3 (Figure 1). As for model intercomparisons, INTER1 is saltier west of  $25^\circ\text{W}$  and slightly less salty between  $10^\circ\text{W}$  and  $25^\circ\text{W}$  within and north of the reservoir compared to CLIM1 (Figures 3e and 3f). Overall, the main characteristics of the tongue remain close to the characteristics of the observed tongue in both simulations, and we consider the model suitable to investigate MOW variability.

### 4.2. Analysis of Modeled MOW Variability in the Gulf of Cadiz

[18] To verify that the difference between the salinity fields in CLIM1 and INTER1 is caused by circulation changes (via the different atmospheric forcing fields) and

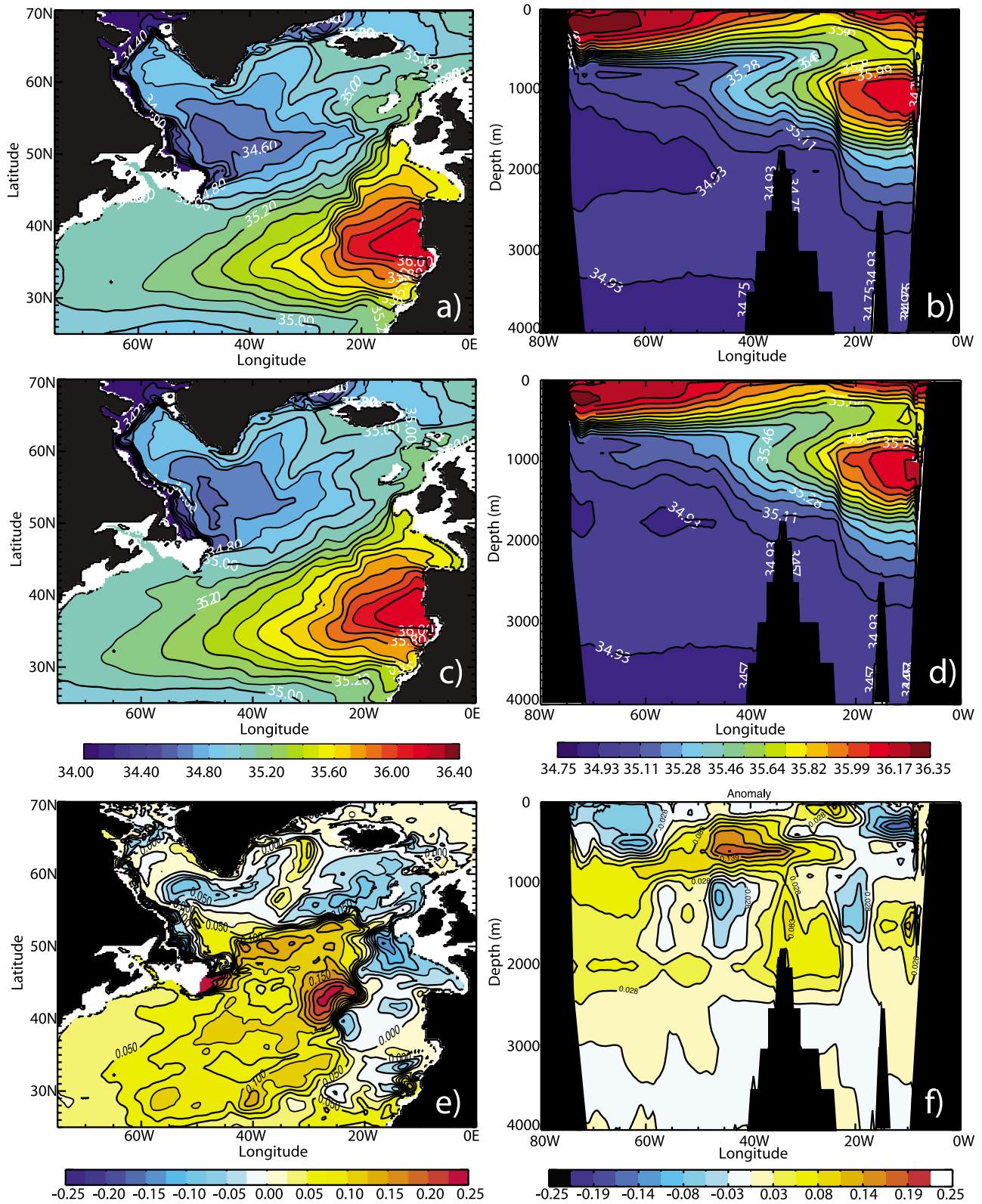


**Figure 3.** Salinity averaged on layers 14 and 15 ( $\sigma_2 = 36.38 \text{ kg/m}^3$  and  $\sigma_2 = 36.52 \text{ kg/m}^3$ ) and over the 59 years of simulation for (a) CLIM1 and (c) INTER1. Vertical salinity section at 36°N for (b) CLIM1 and (d) INTER1. Difference between INTER1 and CLIM1 on (e) layer 14 and on (f) the 36°N vertical section.

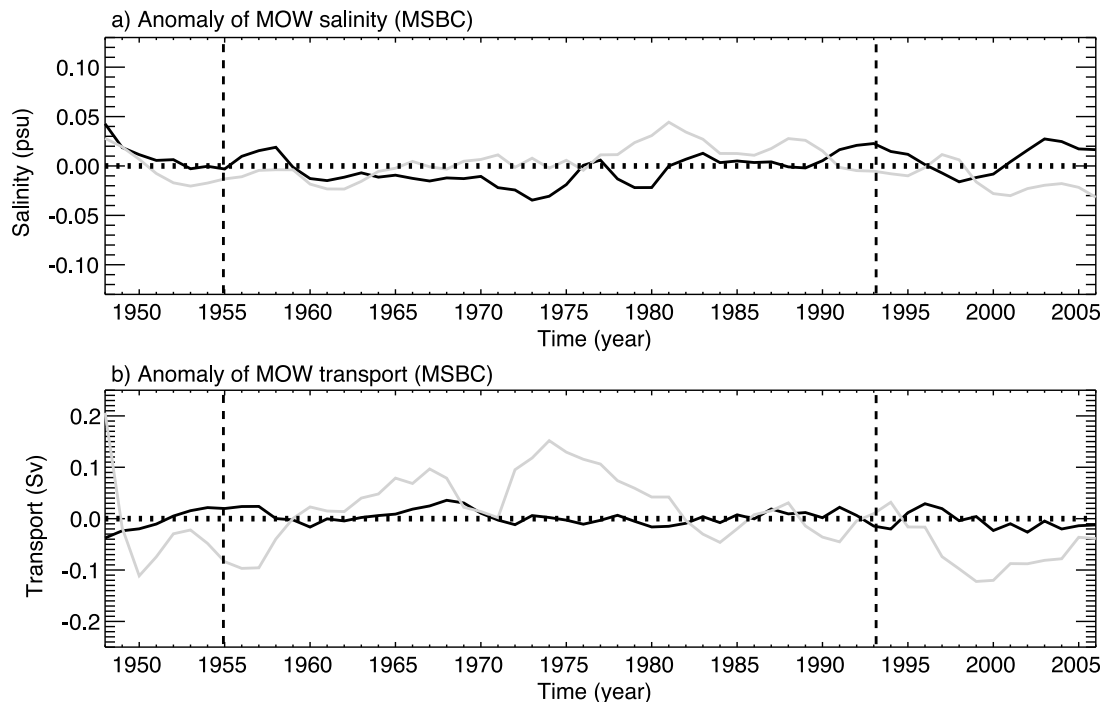


**Figure 4.** (a) Evolution of the anomaly of salinity of the MOW calculated by the MSBC model for CLIM1 (black) and INTER1 (light gray). (b) Evolution of the anomaly of the MOW transport for CLIM1 and INTER1. The subtracted mean used for the anomaly is the mean for the PL04 period (1955–1993) represented by the vertical dashed lines.

not by a difference in MOW properties at the exit of the Gulf of Cadiz ( $S_{out}$ ,  $Tr_{out}$ ), we compare CLIM1 and INTER1 MOW property and transport variability at the exit of the Gulf of Cadiz. Since MOW properties are density compensated, the focus here is on salinity alone (Figure 4).

[19] An inspection of the modeled MOW salinity anomalies at the exit of the Gulf of Cadiz (Figure 4a) shows that CLIM1 anomalies are small throughout the simulation with a slightly positive trend of  $+0.0079 \pm 0.002$  psu/decade ( $r^2 = 0.36$ ). In order to calculate the trend in INTER1, CLIM1 drift is subtracted from the INTER1 time series. As a result, INTER1 MOW anomaly time series has a trend close to zero for the period 1955–1993 ( $+0.0007 \pm 0.002$  psu/decade;  $r^2 = 0.01$ ).

[20] Since variations of MOW transport ( $Tr_{out}$ ) can potentially affect the amount of salt imported into the reservoir, we examine the time evolution of the MOW transport out of the MSBC model (Figure 4b). The modeled MOW transport anomaly in CLIM1 is stable and close to zero throughout the simulation ( $-0.0042 \pm 0.002$  Sv/decade;  $r^2 = 0.10$ ). In INTER1, the modeled MOW transport anomaly varies between  $\pm 0.15$  Sv but shows a trend close to zero as in CLIM1 ( $+0.0067 \pm 0.0088$  Sv/decade;  $r^2 = 0.02$ ; detrended from CLIM1). While there is not so much difference in the T/S variability of MOW at the exit of the Gulf of Cadiz between CLIM1 and INTER1, the impact of interannual atmospheric forcing on MOW is revealed in the variability of the modeled MOW transport.

[21] In summary, we find that the modeled trends for MOW salinity and transport in the Gulf of Cadiz are sufficiently small to be considered stable. Though these trends have been compared to observed changes in this section, we

next show that they are small relative to the changes of the model's MOW reservoir properties.

#### 4.3. MOW Variability in the Reservoir: Observed and Modeled

[22] To ensure that we reproduce the observed MOW variability in this North Atlantic configuration of HYCOM, we calculate the observed and modeled salinity, temperature, and density trends over the spatial domain defined by  $10^\circ\text{W}$  to  $25^\circ\text{W}$  and  $32^\circ\text{N}$  to  $42^\circ\text{N}$  (box 1, Figure 1), considered to be the reservoir for MOW. This spatial domain is slightly altered from that used by PL04 in order to accommodate the slightly larger spread of MOW in the model. The larger MOW spreading area in the model can be attributed to the  $\sim 4$  Sv outflow transport, which is in the upper part of the observed range (3–4 Sv according to *Baringer and Price* [1997]).

[23] Following the same method used by PL04, the observed salinity trend is calculated from the mid-depth maximum salinity anomaly of each profile averaged over box 1. The temperature and density trends are computed from anomalies corresponding to these mid-depth maximum salinity anomalies (Figure 5). The salinity, temperature, and density are extracted using 2293 profiles from the hydrographic database HYDROBASE 2 [*Curry, 2001; Lozier et al., 1995*] for the periods 1955–1993 and 1955–2003 (N.B. The number of observations available over the region between 2003 and 2006 was not sufficient to estimate the trend between 1955 and 2006). The trends for the observed properties and for the property fields from each simulation of this study are summarized in Tables 2 and 3. The obser-

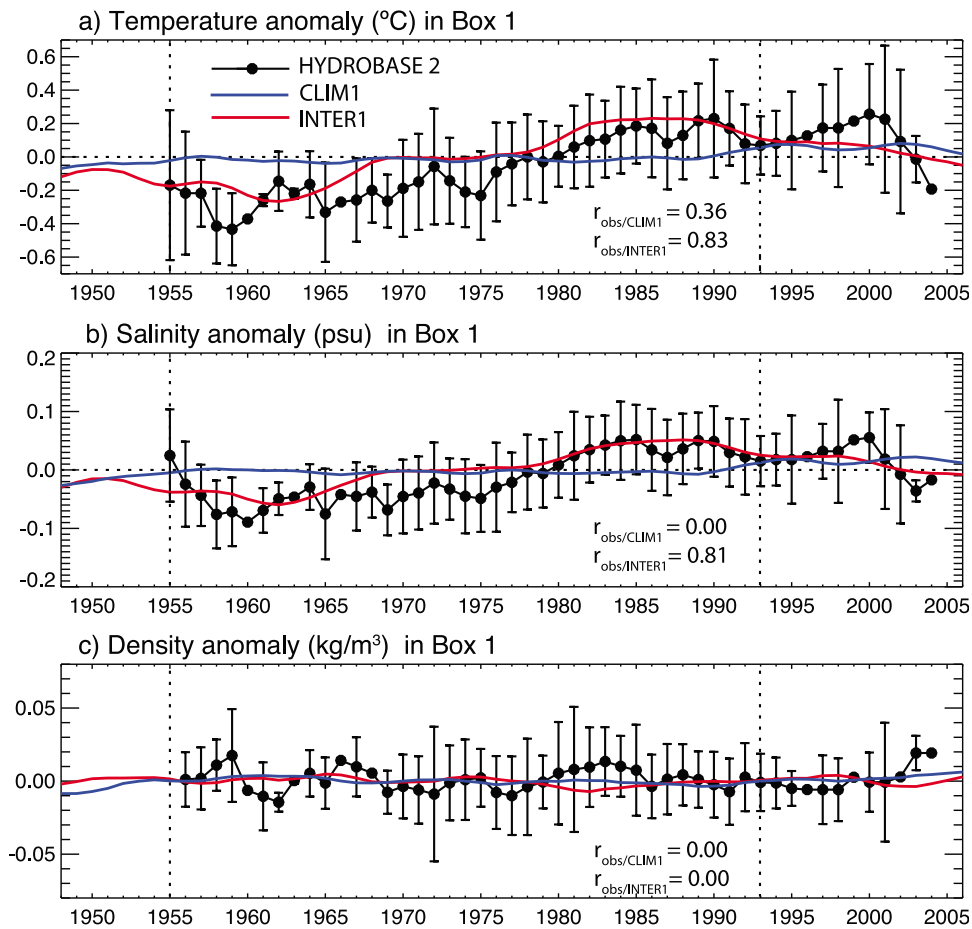


**Figure 5.** Evolution of the anomaly of (a) salinity, (b) temperature, and (c) density for CLIM1 (blue) and INTER1 (red) and HYDROBASE 2 (black) averaged over box 1 [ $10^{\circ}\text{W}$ ,  $25^{\circ}\text{W}$ ,  $32^{\circ}\text{N}$ ,  $42^{\circ}\text{N}$ ]. The subtracted mean used for the anomaly is the mean for the PL04 period (1955–1993) represented by the vertical dashed lines. Correlation ( $r$ ) between observations and model simulations are given for each property. INTER1 correlation is calculated using the INTER1 time series with the CLIM1 trend subtracted.

vational trends in box 1 are comparable to the trends found by PL04 for the period 1955–1993, with a salinity trend of  $0.0337 \pm 0.0032$  psu/decade ( $r^2 = 0.76$ ) and a temperature trend of  $0.155 \pm 0.013^{\circ}\text{C}/\text{decade}$  ( $r^2 = 0.81$ ). Considering the period 1955–2003, we find significantly lower salinity and temperature trends of  $0.0240 \pm 0.0026$  psu/decade ( $r^2 = 0.65$ ) and  $0.119 \pm 0.011^{\circ}\text{C}/\text{decade}$  ( $r^2 = 0.72$ ), respectively, consistent with the freshening observed in 2005 by *Leadbetter et al.* [2007].

[24] The MOW properties in CLIM1 are quite stable for 40 years after the 30-year spin-up. However, the salinity and temperature slightly increase for the last 20 years of the simulation (Figures 5a and 5b). The drift of the model between years 37 and 75 of CLIM1 (corresponding to year 1955 and year 1993 in INTER1) corresponds to a trend of  $0.0004 \pm 0.0006$  psu/decade ( $r^2 = 0.01$ ) for the salinity and  $0.0082 \pm 0.0025^{\circ}\text{C}/\text{decade}$  ( $r^2 = 0.22$ ) for the temperature. These drifts are subtracted from the property time series of INTER1.

**Table 2.** Salinity, Temperature, and Density Trends at 1100 m Between 1955 and 1993 in Box 1 Using the Hydrographic Profiles of HYDROBASE 2 and the Results of CLIM1, INTER1, CLIM2, WIND, and INTER2 Experiments<sup>a</sup>

Experiments	Salinity Trend (psu/decade)	Temperature Trend ( $^{\circ}\text{C}/\text{decade}$ )	Density Trend ( $\text{kg/m}^3/\text{decade}$ )
HYDROBASE2 (Observations)	$0.0337 \pm 0.0032$ ( $r^2 = 0.76$ )	$0.155 \pm 0.013$ ( $r^2 = 0.81$ )	$0.0002 \pm 0.0011$ ( $r^2 = 0.00$ )
CLIM1	$0.0004 \pm 0.0006$ ( $r^2 = 0.01$ )	$0.008 \pm 0.003$ ( $r^2 = 0.22$ )	$-0.0012 \pm 0.0002$ ( $r^2 = 0.46$ )
INTER1	$0.0287 \pm 0.0019$ ( $r^2 = 0.86$ )	$0.125 \pm 0.009$ ( $r^2 = 0.82$ )	$0.0001 \pm 0.0003$ ( $r^2 = 0.00$ )
CLIM2	$0.0082 \pm 0.0018$ ( $r^2 = 0.37$ )	$0.034 \pm 0.006$ ( $r^2 = 0.75$ )	$0.0003 \pm 0.0007$ ( $r^2 = 0.05$ )
WIND	$0.0117 \pm 0.0011$ ( $r^2 = 0.74$ )	$0.052 \pm 0.007$ ( $r^2 = 0.63$ )	$-0.0001 \pm 0.0004$ ( $r^2 = 0.00$ )
INTER2	$0.0237 \pm 0.0024$ ( $r^2 = 0.72$ )	$0.092 \pm 0.013$ ( $r^2 = 0.59$ )	$0.0021 \pm 0.0011$ ( $r^2 = 0.09$ )

<sup>a</sup>INTER1, WIND, and INTER2 results are calculated removing the drift found in CLIM1 or CLIM2.

**Table 3.** Same as Table 2 but for 1955–2003

Experiments	Salinity Trend (psu/decade)	Temperature Trend ( $^{\circ}\text{C}/\text{decade}$ )	Density Trend ( $\text{kg}/\text{m}^3/\text{decade}$ )
HYDROBASE2 (Observations)	$0.024 \pm 0.0026$ ( $r^2 = 0.65$ )	$0.119 \pm 0.011$ ( $r^2 = 0.72$ )	$0.000 \pm 0.0001$ ( $r^2 = 0.00$ )
CLIM1	$0.0039 \pm 0.0007$ ( $r^2 = 0.42$ )	$0.019 \pm 0.002$ ( $r^2 = 0.58$ )	$-0.0003 \pm 0.0002$ ( $r^2 = 0.04$ )
INTER1	$0.0133 \pm 0.0022$ ( $r^2 = 0.45$ )	$0.060 \pm 0.010$ ( $r^2 = 0.42$ )	$-0.0002 \pm 0.0003$ ( $r^2 = 0.01$ )
CLIM2	$0.0079 \pm 0.0011$ ( $r^2 = 0.50$ )	$0.037 \pm 0.005$ ( $r^2 = 0.59$ )	$-0.0005 \pm 0.0004$ ( $r^2 = 0.02$ )
WIND	$0.0090 \pm 0.0009$ ( $r^2 = 0.67$ )	$0.049 \pm 0.005$ ( $r^2 = 0.72$ )	$-0.0018 \pm 0.0005$ ( $r^2 = 0.25$ )
INTER2	$0.0131 \pm 0.0023$ ( $r^2 = 0.41$ )	$0.047 \pm 0.010$ ( $r^2 = 0.30$ )	$0.0020 \pm 0.0007$ ( $r^2 = 0.14$ )

[25] INTER1 properties exhibit significant variations compared with those of CLIM1. The salinity and temperature anomalies first decrease from 1948 to 1962 ( $-0.05$  psu and  $-0.25^{\circ}\text{C}$ ) and then increase from 1962 to 1982 ( $+0.05$  psu and  $+0.2^{\circ}\text{C}$ ) when both properties stabilize for 8–9 years. INTER1 properties then decrease again until the end of the simulation in 2006. Negligible density variation occurs during the simulation. The salinity trend,  $0.0287 \pm 0.0019$  psu/decade ( $r^2 = 0.86$ ) matches the observed trend within error while the temperature trend,  $0.125 \pm 0.009^{\circ}\text{C}/\text{decade}$  ( $r^2 = 0.82$ ), is slightly lower. For both time series, over 80% of the variance is explained by the linear trend. Furthermore, the modeled salinity and temperature fields in INTER1 are highly correlated with the observed values, with correlation coefficients of 0.81 and 0.83, respectively. There are only negligible correlations between CLIM1 properties and the observations. Thus, the modeled MOW in INTER1 reproduces the observed MOW trend and the interannual variability with a fair degree of skill for the period 1955–1993. This result implies that North Atlantic circulation changes are sufficient to explain observed MOW variability between 1955 and 1993. A summary of the salinity, temperature and density trends for each experiment and time period is given in Tables 2 and 3.

[26] Between 1955 and 2003, the model drift (in CLIM1) is slightly larger than between 1955 and 1993 with  $0.0003 \pm 0.0007$  psu/decade for the salinity and  $0.019 \pm 0.002^{\circ}\text{C}/\text{decade}$  for the temperature. The corresponding trends for INTER1 with the drift removed are  $0.0133 \pm 0.0022$  psu/decade for the salinity and  $0.060 \pm 0.01^{\circ}\text{C}/\text{decade}$  for the temperature. These

trends are in agreement with the variability of MOW properties described by *Leadbetter et al.* [2007]. Indeed, comparing  $\Theta/S$  profiles (potential temperature/salinity) of INTER1 averaged between  $10^{\circ}\text{W}$  and  $20^{\circ}\text{W}$  at  $36^{\circ}\text{N}$  with the profiles of *Leadbetter et al.* [2007] for 1959, 1981, and 2005 (Figure 6), we see that the simulation reproduces the warming and salinification between 1959 and 1981 and the cooling and freshening between 1981 and 2005.

[27] In summary, the observed MOW reservoir variability is successfully reproduced over the last 59 years without property and/or transport changes of the source water from the Mediterranean Sea. Instead, the variable MOW properties are attributed to ocean circulation changes that result from interannually varying atmospheric forcing alone. In the second part of this study, we investigate the impact of each component of the atmospheric forcing (i.e., wind stress and buoyancy fluxes) on the MOW and describe the mechanisms responsible for MOW variability and its pathways over the past decades.

## 5. Description of the Mechanism Driving the MOW Variability

[28] Three simulations of 59 years are performed starting from year 30 of CLIM1 described in section 4. CLIM2, the control simulation, is forced by the climatological forcing ERA15. The WIND simulation is forced with the NCEP/NCAR interannual wind stress over the period 1948–2006 and the climatological buoyancy forcing from ERA15. The INTER2 simulation is forced with the interannual NCEP/

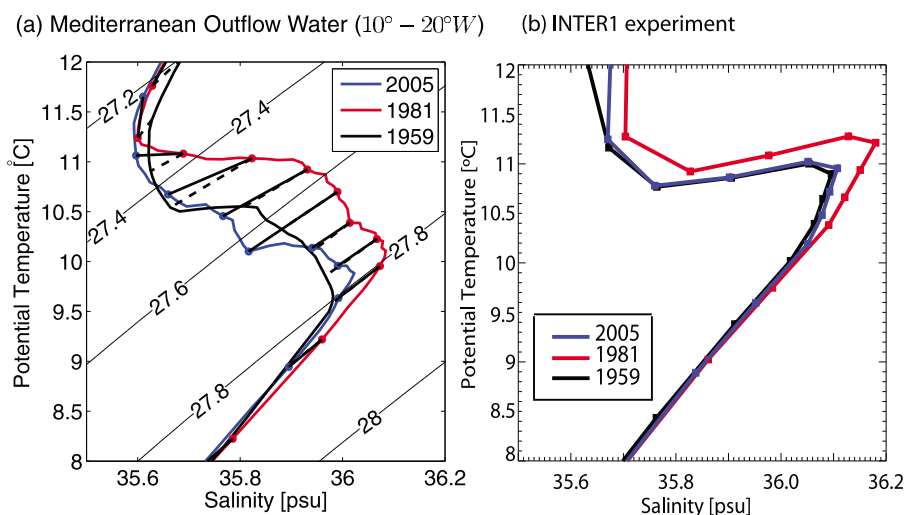


**Figure 6.** Mean  $\theta/S$  profiles of a repeated section (1959 in black, 1981 in red, and 2005 in blue) at  $36^{\circ}\text{N}$  between  $10^{\circ}$ – $20^{\circ}\text{W}$  at the depth of the MOW (a) from *Leadbetter et al.* [2007] and (b) for INTER1.

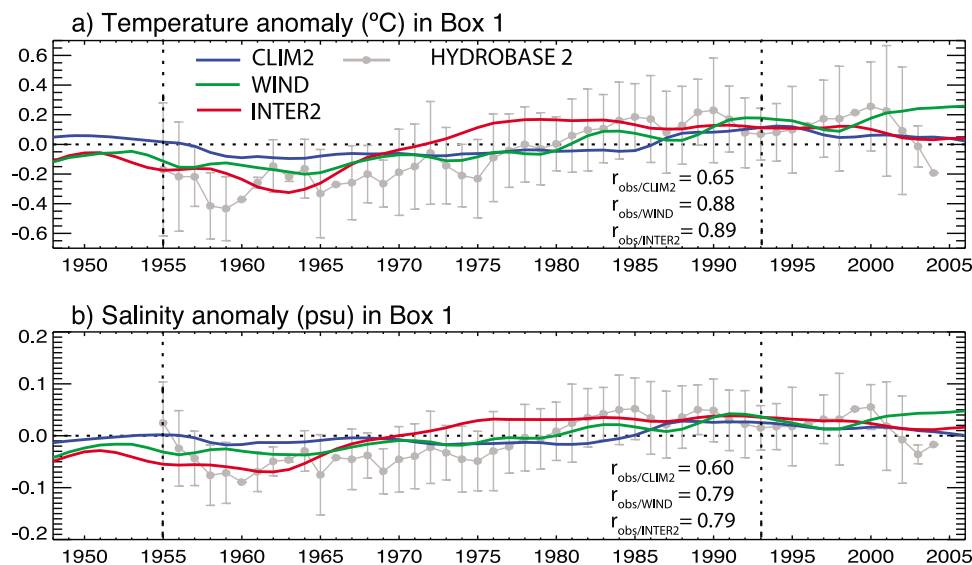


**Figure 7.** Evolution of the anomaly of salinity and temperature in box 1 (Figure 1) for CLIM2 (blue), WIND (green), INTER2 (red) and HYDROBASE 2 (light gray). The subtracted mean used for the anomaly is the mean for the PL04 period (1955–1993) represented by the vertical dashed lines. Correlation ( $r$ ) between observations and model simulations are given for each property. WIND and INTER2 correlations are calculated using WIND and INTER2 time series with the CLIM2 trend subtracted.

NCAR wind stress and buoyancy forcing (see Table 1). Since the variability of the MOW at the exit of the Gulf of Cadiz does not contribute to the MOW variability in the Atlantic (see section 4.3), we prescribe a constant property Mediterranean outflow at  $8.3^\circ\text{W}$  in the Gulf of Cadiz equal to the average values of the MSBC MOW salinity, temperature, and transport of the climatological experiment CLIM1:  $S = 36.2$  psu,  $T = 11^\circ\text{C}$ , and the total transport  $Tr = 4$  Sv ( $1 \text{ Sv} = 10^6 \text{ m}^3/\text{s}$ ). The MOW is “injected” into HYCOM in layers 14 and 15, corresponding to the target densities  $\sigma_2 = 36.38 \text{ kg/m}^3$  and  $\sigma_2 = 36.52 \text{ kg/m}^3$ , in which MOW is neutrally buoyant.

### 5.1. Comparison of Observed and Modeled MOW Variability

[29] As in section 4.3, to see if the model reproduces the observed trends in the reservoir in this North Atlantic configuration of HYCOM, we calculate the modeled salinity, temperature, and density trends over box 1 (Figure 7).

[30] The trends for the observed properties and for the property fields from each of the three simulations discussed above are summarized in Tables 2 and 3, for the time periods 1955–1993 and 1955–2003, respectively. CLIM2 has a slight model drift of  $0.0082 \pm 0.0018$  psu/decade ( $r^2 = 0.37$ ) for the salinity and  $0.034 \pm 0.007^\circ\text{C}/\text{decade}$  ( $r^2 = 0.75$ ) for the temperature between year 7 and 45, corresponding to year 1955 and 1993 in the interannual runs. The drift between year 7 and 55 (1955–2003) is comparable (see Table 3). As in sections 4.2 and 4.3, these drifts are subtracted from the appropriate time series with variable forcing.

[31] WIND has a salinity (temperature) trend of  $0.0117 \pm 0.0011$  psu/decade ( $0.052 \pm 0.007^\circ\text{C}/\text{decade}$ ) over the time period 1955–1993, weaker than the observed trend by approximately half. During 1955–2003, the WIND salinity (temperature) trend remains close to its 1955–1993 trend

with  $0.0090 \pm 0.0009$  psu/decade ( $0.049 \pm 0.005^\circ\text{C}/\text{decade}$ ). In contrast, the INTER2 salinity (temperature) trend is  $0.0237 \pm 0.0024$  psu/decade ( $0.093 \pm 0.013^\circ\text{C}/\text{decade}$ ) for the 1955–1993 period and  $0.0131 \pm 0.0023$  psu/decade ( $0.047 \pm 0.010^\circ\text{C}/\text{decade}$ ) for 1955–2003. The INTER2 trends are somewhat weaker than the observed trends ( $\sim 71\%$  and  $55\%$  of the salinity trends for 1955–1993 and 1955–2003, respectively), yet significantly closer to the observations than CLIM2 or WIND. As with INTER1, a significant portion of the variance in the INTER2 and WIND property time series is explained by the linear trends. For the remainder of the paper, we assume that the match between INTER2 and the observed property changes is sufficient to further use this simulation. Furthermore, from this analysis, we conclude that both an interannually varying wind stress and an interannually varying buoyancy forcing are necessary to reproduce the observed MOW trend in the reservoir.

### 5.2. Evolution of the MOW Salinity Pattern

[32] To investigate further the MOW reservoir variability reproduced in INTER2, the MOW salinity pattern during the period when INTER2 exhibits relatively low salinity (1955–1970) is compared to the salinity pattern during the period when INTER2 exhibits relatively high salinity (1980–1995) (Figure 8). For both of these time periods the salinity is averaged on layers 14 and 15 ( $\sigma_2 = 36.38 \text{ kg/m}^3$  and  $\sigma_2 = 36.52 \text{ kg/m}^3$ ), the layers in which MOW is introduced into HYCOM.

[33] The comparison of CLIM2 salinity patterns between the two periods (Figures 8a and 8d) shows a freshening west of  $30^\circ\text{W}$  and a salinification south of  $30^\circ\text{N}$  (Figure 8g), illustrating the drift of the model between these two periods. As seen in Figures 8b, 8e, and 8h, the evolution of the WIND salinity pattern is similar to the evolution in CLIM2,

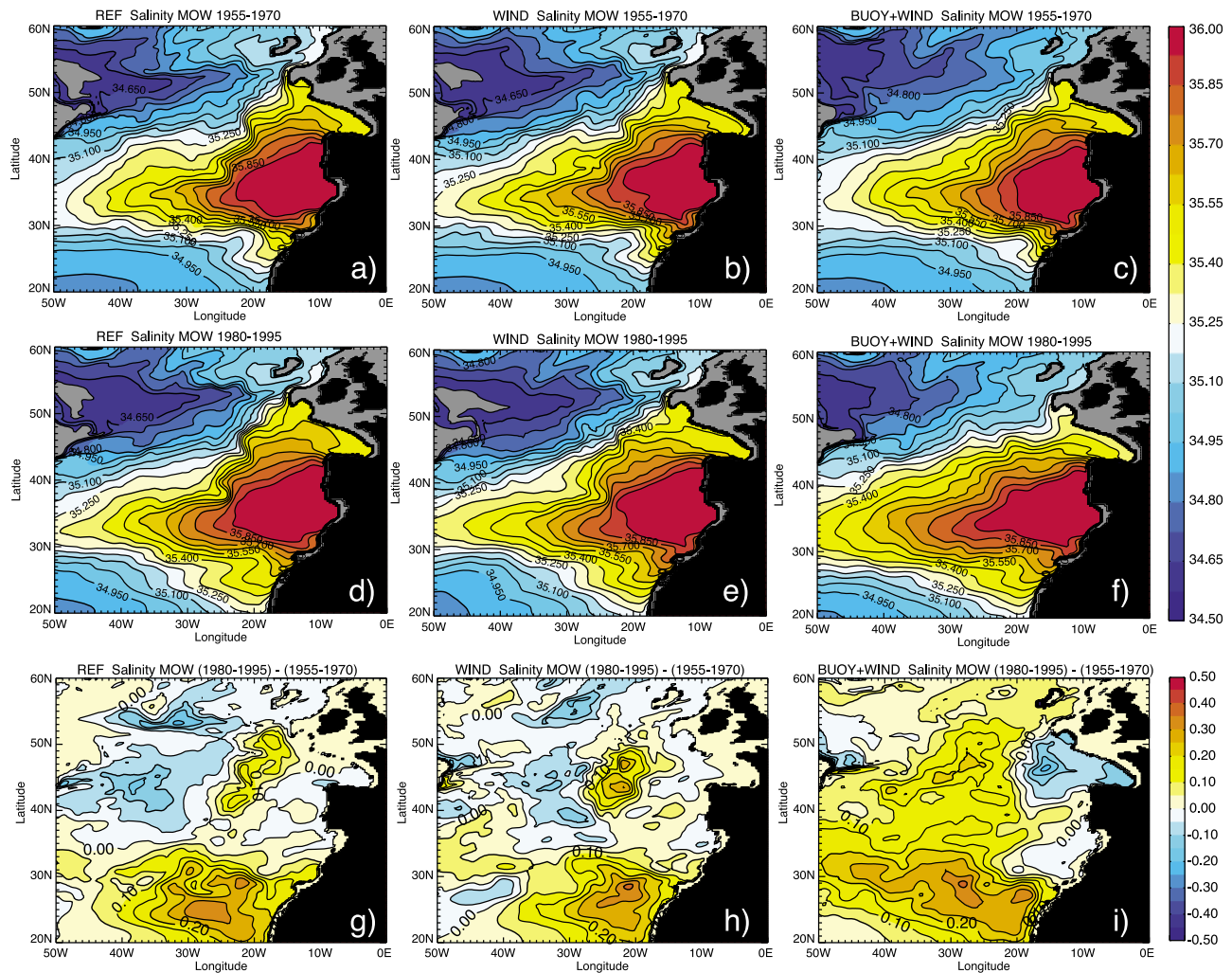


**Figure 8.** Salinity of averaged over  $\sigma_2 = 36.38 \text{ kg/m}^3$  and  $\sigma_2 = 36.52 \text{ kg/m}^3$  for (left) CLIM2, (middle) WIND, and (right) INTER2 averaged over the periods (a–c) 1955–1970 and (d–f) 1980–1995 and the (g–i) difference of salinity between these two periods.

with the exception of a more accentuated salinification in the region from 20 to 30°W and 40–50°N. In INTER2, there are notable differences from CLIM2 and WIND. While the salinification south of 30°N in the control simulation is also present in this model configuration (Figure 8i), albeit stronger, the freshening west of 30°W is not. On the contrary, we find a widespread salinification in the central and western portions of the basin. This salinification is readily apparent in the extension of the MOW tongue from the earlier to the latter time period: the western extent of the MOW tongue (as measured by the 35.9 psu isohaline) is located near 20°W during 1955–1970, yet at 27°W during 1980–1995 (Figures 8c and 8f). Such an extension is not apparent in the CLIM2 and WIND fields. The salinification in the INTER2 fields finds an exception only near the extended regions of the Gulf of Cadiz and the Bay of Biscay, where freshening is noted, especially for the latter region. Given these strong features, we conjecture that the salinification in the west and freshening in the north (in the Bay of Biscay) are due to a westward expansion of the tongue and consequently its retraction from the north. This mechanism

can be described as a shift of the MOW pathway from north to west. This possibility is pursued in the following sections.

### 5.3. Evolution of the Transport in Box 1

[34] To ascertain whether an MOW pathway shift occurred between 1955 and 1970 and 1980–1995, we analyze the evolution of the transports at each boundary of box 1 (Figure 9). The transport is positive for water flowing out of the box and is calculated for layers 14 and 15. In all cases, the transport at the eastern boundary of box 1 is close to the 4 Sv prescribed as MOW transport. The balance to this input is achieved by a combination of output from the northern, southern and western boundaries. Importantly, these outputs vary with each model run, as described below.

[35] The outgoing transports in box 1 in the climatological simulation CLIM2 are relatively stable throughout the simulation. The northern boundary transport is dominant (with an average of +2.17 Sv); the southern and western boundary transports are close to zero except during 1950–1955 and 1985–2005, when the western boundary transport is  $\sim +1$  Sv. In WIND, the transports exhibit larger variations than in CLIM2. The northern boundary transport is also the

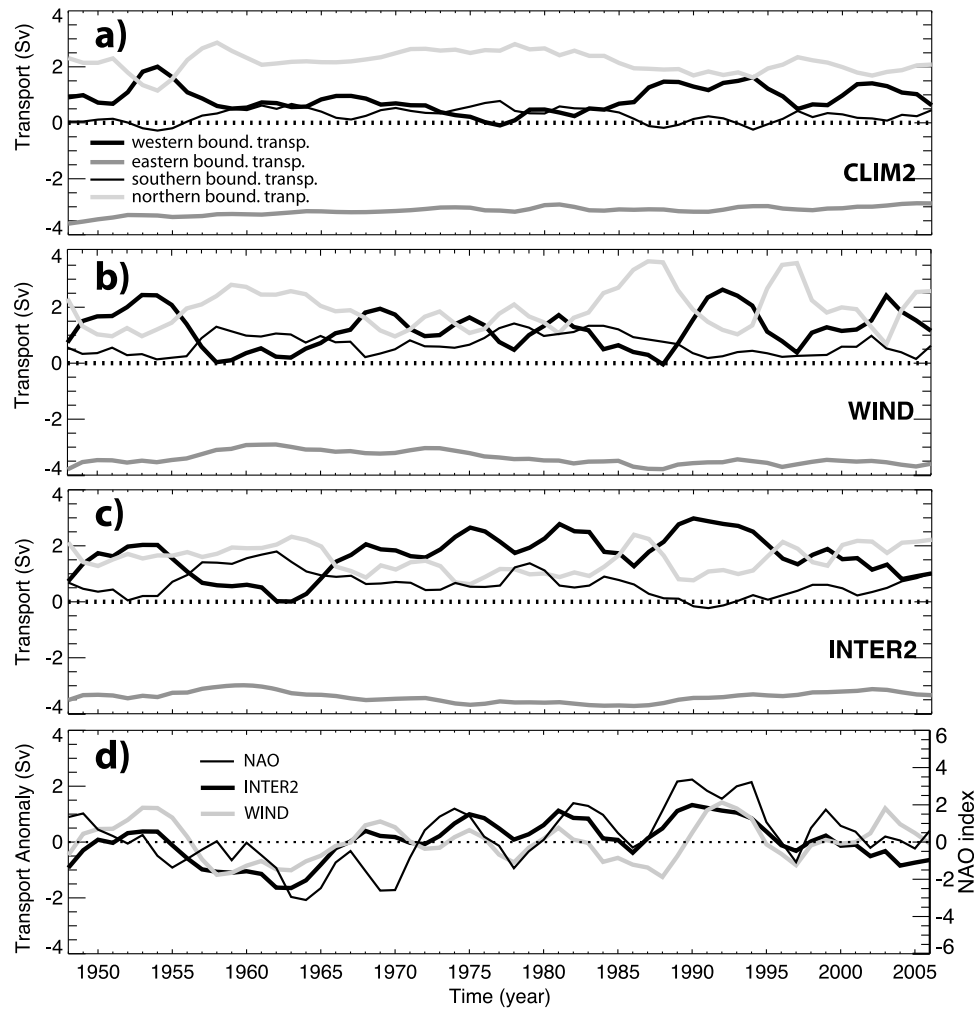


**Figure 9.** (a–c) Transport budget in box 1 (see Figure 1) for each experiment: transport at the eastern boundary (dark gray), at the western boundary (thick black), at the northern boundary (light gray) and at the southern boundary (thin black). Transports are positive for a flow going out of the box. (d) The anomaly of western boundary transport for WIND (light gray) and INTER2 (thick black) with the winter NAO index [Hurrell, 1995] superimposed in thin black.

dominant transport for most of the simulation, with an average of +1.93 Sv compared with an average of +1.20 Sv for the western boundary transport. Occasionally, the western boundary transport has a stronger intensity than the northern boundary transport (i.e., during 1950–1955 and 1990–1995). Furthermore, WIND presents a significant anti-correlation between its western and northern boundary transports ( $r = 0.80$ ,  $p < 0.01$  at lag 0). In INTER2, the averages of the northern and western boundary transports are roughly equivalent over the period of the simulation, at +1.51 Sv and +1.65 Sv, respectively. The northern boundary transport is dominant during the 1955–1965 period and after 1995; and the western boundary transport is generally dominant during 1970–1995. Furthermore, as with WIND, the transports at the northern and western boundaries are strongly anti-correlated ( $r = 0.79$ ;  $p < 0.01$  at lag 0). These results indicate that MOW has preferred pathways (northward or westward) that are temporally variable as seen in WIND and INTER2 and that the dominant MOW pathway has varied between 1948 and 2006.

[36] To understand how variability of the transport relates to variability of the atmospheric forcing, we calculate the correlation of each transport with the dominant mode of North Atlantic atmospheric variability: the winter North Atlantic Oscillation index (NAO) [Hurrell, 1995]. In INTER2, the NAO index is significantly correlated with the western boundary transport at lag 0 ( $r = 0.65$ ;  $p < 0.01$ ) and significantly anti-correlated with the northern boundary transport at lag 0 ( $r = 0.45$ ;  $p < 0.01$ ). Thus, MOW has a tendency to spread northward during low NAO and westward during high NAO, explaining the salinification in the west and the freshening in the north in the 1980–1995 period compared with the 1955–1970 period. Furthermore, the variability of the western/northern boundary transport in INTER2 is correlated/anticorrelated with the salinity variability in box 1 ( $r = 0.72/-0.45$ ;  $p < 0.01$ ), supporting our conjecture that shifts in the dominant pathway are responsible for the salinity trend in box 1 observed between 1955 and 2003. As evident in Figure 9, WIND transports are significantly correlated with INTER2 transports ( $r =$

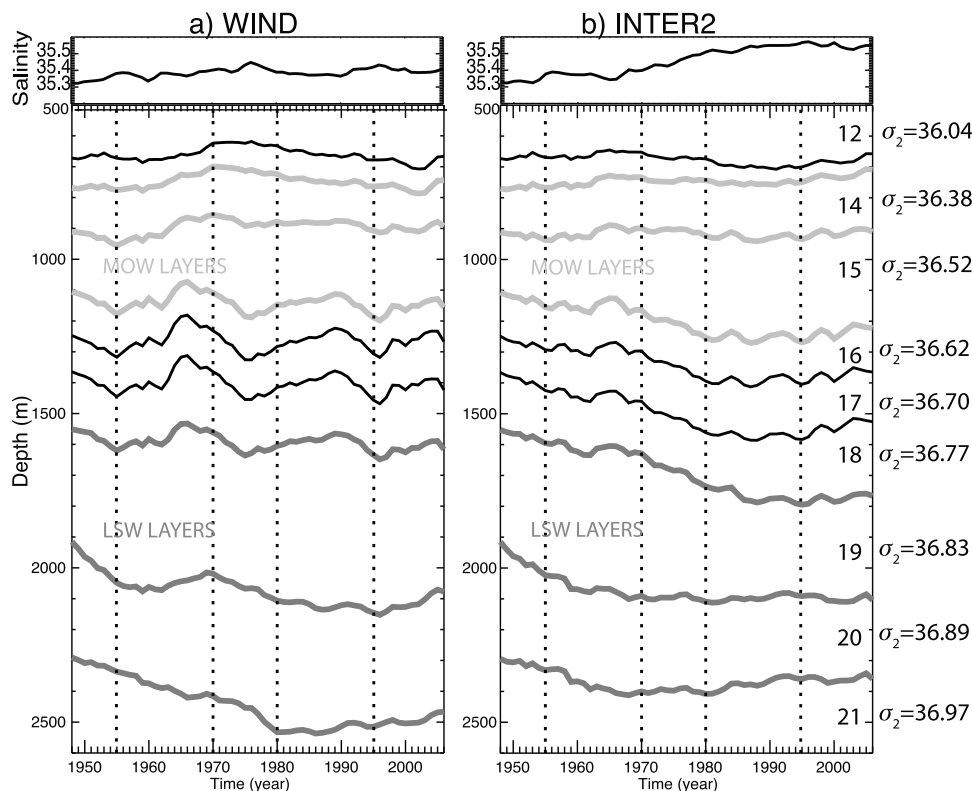


**Figure 10.** Time evolution of the thickness of ten density classes ranging from  $\sigma_2 = 36.04 \text{ kg/m}^3$  and  $\sigma_2 = 36.97 \text{ kg/m}^3$  averaged over box 2 for (a) WIND and (b) INTER2. The evolution of salinity averaged over the same region for the two MOW density classes is given on top. The evolution of the MOW density classes is in light gray while the evolution of the LSW density classes is in dark gray. Vertical dotted lines bounds the period 1955–1970 and 1980–1995. The number of the layer and their corresponding densities is given on the right panel.

0.70/0.65;  $p < 0.01$  for the northern/western boundary transports), indicating that the pathway shifts in INTER2 are primarily wind-induced. Interestingly, the WIND transports are not significantly correlated with the NAO index or with the salinity in box 1, suggesting in the former case that the full forcing field (wind and buoyancy) is needed to most closely capture the broad variability measured by the NAO index. The latter case suggests that although the mechanical impact of the time varying wind stress induces an anti-correlation between the northern and western boundary transport, time-varying buoyancy forcing is needed to reproduce the observed MOW property variability.

#### 5.4. Impacts of the Pathway Shifts

[37] We next investigate the impact of these pathway shifts on the distribution of MOW in the North Atlantic. We include changes in the thickness and spread of Labrador Sea Water (LSW) in this investigation since LSW and MOW constitute the two major mid-depth water masses in the North Atlantic and the salinity field at mid-depth is intricately linked to the distribution of both of these water masses. Also in the section, the consequences for MOW variability in the Rockall Trough are analyzed.

##### 5.4.1. Variability of MOW Along the Western Pathway

[38] A comparison of the water mass distribution of WIND and INTER2 in the central Atlantic is conducted in the region where the MOW tongue expands to the west of

box 1 [ $30^\circ\text{W}$ ,  $40^\circ\text{W}$ ,  $30^\circ\text{N}$ ,  $40^\circ\text{N}$ ] (box 2, Figure 1). The thickness evolution of each density class between 500 m and 2600 m (here corresponding to ten density classes from  $\sigma_2 = 36.04 \text{ kg/m}^3$  to  $\sigma_2 = 36.97 \text{ kg/m}^3$ ) is calculated (Figure 10).

[39] WIND shows weak variability in layer thickness in every density class, except for the LSW densities ( $\sigma_2 = 36.83 \text{ kg/m}^3$  and  $\sigma_2 = 36.89 \text{ kg/m}^3$ ), which exhibit an increase in the 1960s and again in the 1980s (Figure 10a). The salinity in the MOW density classes ( $\sigma_2 = 36.38 \text{ kg/m}^3$  and  $\sigma_2 = 36.52 \text{ kg/m}^3$ ) in this region stays quite stable throughout the simulation (Figure 10a, top). In INTER2, larger variability of the MOW density class thickness ( $\sigma_2 = 36.52 \text{ kg/m}^3$ ) and the LSW density class thickness ( $\sigma_2 = 36.83 \text{ kg/m}^3$ ) (Figure 10b) than in WIND is apparent. The increase in salinity (+0.1 psu) after 1970 in the MOW density classes (Figure 10b, top) indicates that the thickness can indeed be attributed to MOW. We also note that the increase of the MOW density class thickness in the 1980s coincides with a decrease of the LSW density class thickness over the same period. Since the thicknesses of the density classes located between LSW and MOW stay constant throughout the simulation, we suggest that the variability of the LSW and MOW density class thicknesses are connected. This connection is examined in the following section.

##### 5.4.2. LSW Variability and MOW Pathway Shifts

[40] To understand how LSW variability is related to MOW pathway shifts, the evolution of LSW density class thickness

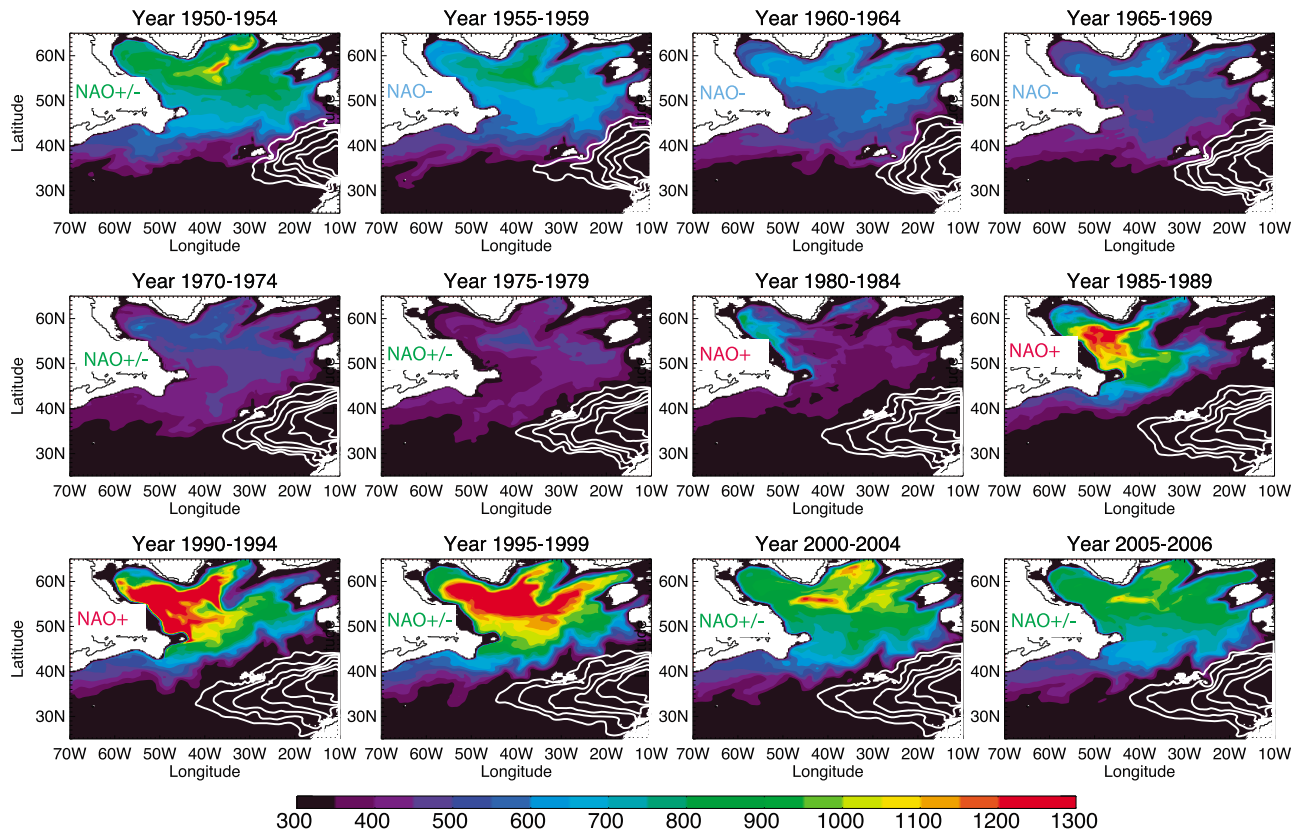


**Figure 11.** Evolution of the LSW density class ( $\sigma_2 = 36.83 \text{ kg/m}^3$ ) thickness (m) by 5-year bin from 1950 to 2006 in INTER2. White contours are salinity contours of the MOW ( $\sigma_2 = 36.52 \text{ kg/m}^3$ ) from 35.7 psu to 36.2 psu. The NAO state is given for each 5-year bin from 1950 to 2004 and for 2005–2006.

over the entire North Atlantic is analyzed concurrently with the evolution of the MOW salinity tongue for twelve intervals of 5 years over our study domain (Figure 11). In INTER2, the LSW density class thickness varies strongly during the nearly 60 years of simulation. At the beginning of the simulation (1950–1954), LSW covers most of the western basin of North Atlantic (north of  $40^\circ\text{N}$ ) and part of the eastern basin except for the region east of  $25^\circ\text{W}$  at the latitude of the Bay of Biscay ( $40^\circ\text{N}$ – $48^\circ\text{N}$ ). The average thickness of the LSW density class is  $\sim 800$  m from  $65^\circ\text{N}$  to  $45^\circ\text{N}$  and decreases to an average thickness of less than 300 m south of  $40^\circ\text{N}$ . At the outset, the MOW tongue is strongly constrained to the eastern part of the basin (white contours). Between 1955 and 1969, NAO is in a negative phase and little to no LSW is formed, therefore, the thickness of the LSW density class constantly decreases during this period, in agreement with observations [Curry *et al.*, 1998]. Between 1955 and 1969, MOW is constrained at the coast but a northward extension of the salinity contours in the northern part of the Bay of Biscay is apparent, in agreement with a preferred northward pathway during low NAO period (see section 5.3).

[41] During intermediate NAO years (1970–1979), LSW density class thickness continues to decrease till it reaches an average of less than 400 m over the northern Atlantic. LSW then starts to retreat from the eastern North Atlantic basin (1975–1979). During that same time period, MOW salinity contours retract from the northern Bay of Biscay and starts to expand westward to the central Atlantic.

[42] The formation of LSW resumes in the high NAO period (1980–1999). Starting with moderate water mass formation during 1980–1984, LSW formation is enhanced during 1985–1999 when the thickness of the water mass reaches more than 1000 m over most of the subpolar gyre region, as observed by Curry *et al.* [1998]. Retreated to the western north Atlantic basin (1985–1989), LSW progressively refills the North Atlantic and reaches the central Atlantic and the eastern basin during 1995–1999. During the high NAO period, MOW salinity continues to expand westward to the central North Atlantic region and the salinity contours are confined to the southern part of Bay of Biscay, consistent with a preferred westward pathway during a high NAO period.

[43] After 1995, NAO is in an intermediate phase; LSW covers most of the northern Atlantic and has an average thickness of  $\sim 800$  m, as it did at the beginning of the simulation. The MOW is still extended westward during this period; however, we notice a slight retreat of the inner salinity contours toward the east, especially after 2000. At the same time, the salinity contours in the Bay of Biscay shows a northward extension as in the low NAO state. This last result shows that the MOW has a preferred northward pathway after 2000, as it did during 1950–1970. Note: the pathway shifts discussed above are consistent with the changes shown in Figure 9.

[44] A similar investigation to that shown in Figure 11 was conducted for WIND, though the results were not sufficiently interesting to show here. In brief, the variability of the LSW density class thickness and spreading area for WIND is

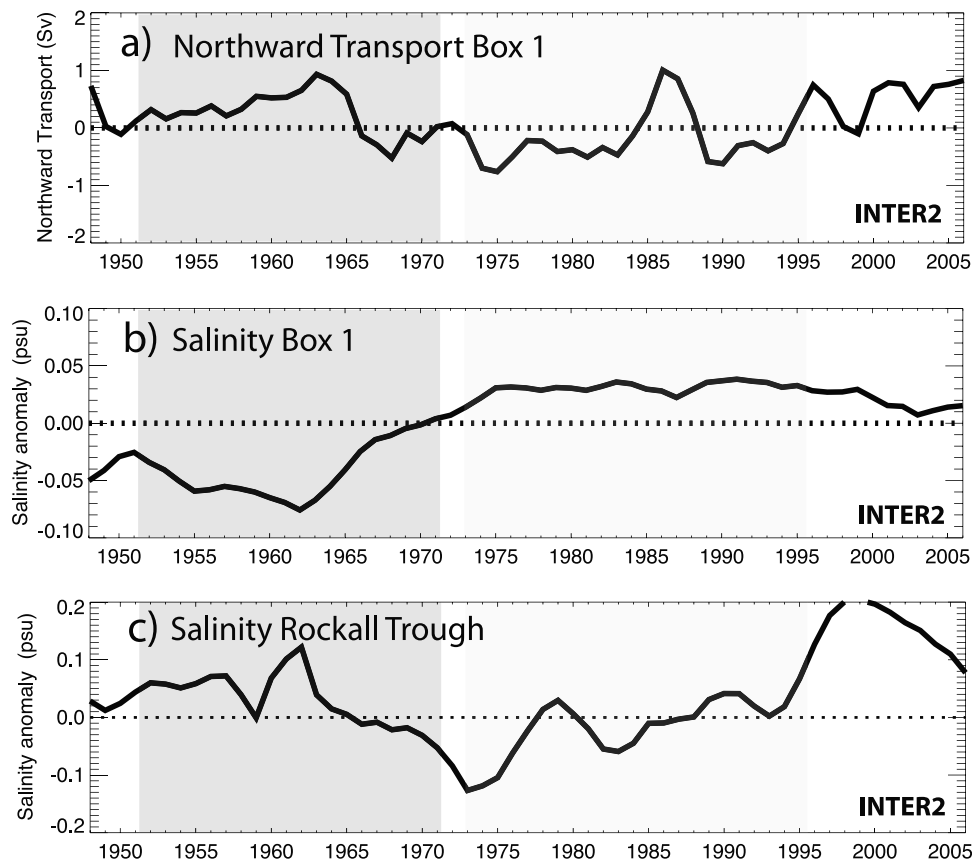


**Figure 12.** Evolution of the 3-year running mean (a) northward transport anomaly, and salinity anomaly (b) in box 1 and (c) in the Rockall Trough (box 3) for INTER2. To highlight the impact of low (dark gray shaded area) and high (light gray shaded area) NAO phases on the MOW circulation, the subtracted mean used for the anomaly is 1955–1995.

weaker than in INTER2. The LSW density class thickness average over the North Atlantic basin have variations from  $\sim 600$  m (1950–1969 and 1990–2006) to  $\sim 900$  m (1970–1989) and the spreading area stays similar to the INTER2 1950–1954 spreading area (Figure 11), except for the last 15 years of simulation when a slight northward displacement of the southeastern boundary (near the box 1 region) occurs. During the simulation, the MOW salinity tongue stays confined to the eastern basin with salinity contours extended northward and occasionally westward, in agreement with the variability of the WIND northern and western boundary transports (see section 5.3).

[45] In sum, though the northern and western pathway shifts are evident in both WIND and INTER2, only INTER2 reproduces a realistic salinity change in the eastern subtropical basin. We conclude that variable buoyancy forcing is necessary to produce the observed properties of the water masses that are affected by these wind-induced pathway shifts. Do these pathway shifts also explain MOW variability along the northern pathway, in particular in the Rockall Trough? This question is next addressed.

#### 5.4.3. Variability of the MOW in the Rockall Trough

[46] The impact of a variable northern pathway is analyzed by calculating the salinity anomaly averaged over the Rockall Trough [ $11.5^{\circ}\text{W}$ ,  $15^{\circ}\text{W}$ ,  $52.5^{\circ}\text{N}$ ,  $57.5^{\circ}\text{N}$ ] (box 3, Figure 1). To highlight the impact of low and high NAO phases on

MOW pathway changes and the subsequent property changes, we calculate the salinity anomaly relative to the mean salinity between 1955 and 1995 for both box 3 and box 1.

[47] In the Rockall Trough, INTER2 salinity anomalies vary from an average of  $\sim +0.05$  psu in the low NAO phase (1950–1970) to an average of  $-0.05$  psu in the high NAO phase (1975–1995) (Figure 12c). During the two periods of consistently low and high NAO (shaded gray in Figure 12), a higher (lower) northward transport is linked to higher (lower) salinities in the Rockall Trough. Indeed, the correlation between the Rockall Trough salinity and the northern transport of box 1 (Figure 12a) during 1948–1995 is positive ( $+0.57$ ) and significant ( $p < 0.01$ ). The correlation between the Rockall Trough salinity and salinity in box 1 (Figure 12b), where the MOW reservoir resides, is negative ( $-0.56$ ) and significant ( $p < 0.01$ ), in agreement with the pathway shift hypothesis.

[48] After 1995, when the NAO index decreases, an expected increase in the northward pathway and decrease in the salinity in box 1 are evident, changes that are consistent with a pathway shift hypothesis. Importantly, the gradual decrease in salinity in box 1 is in agreement with observations [Leadbetter *et al.*, 2007]. However, though the salinity in box 3 (Rockall Trough) initially increases (in agreement with Holliday [2003] and Holliday *et al.* [2008]), it decreases starting in 1999. Thus after 1999, the salinities in box 1 and

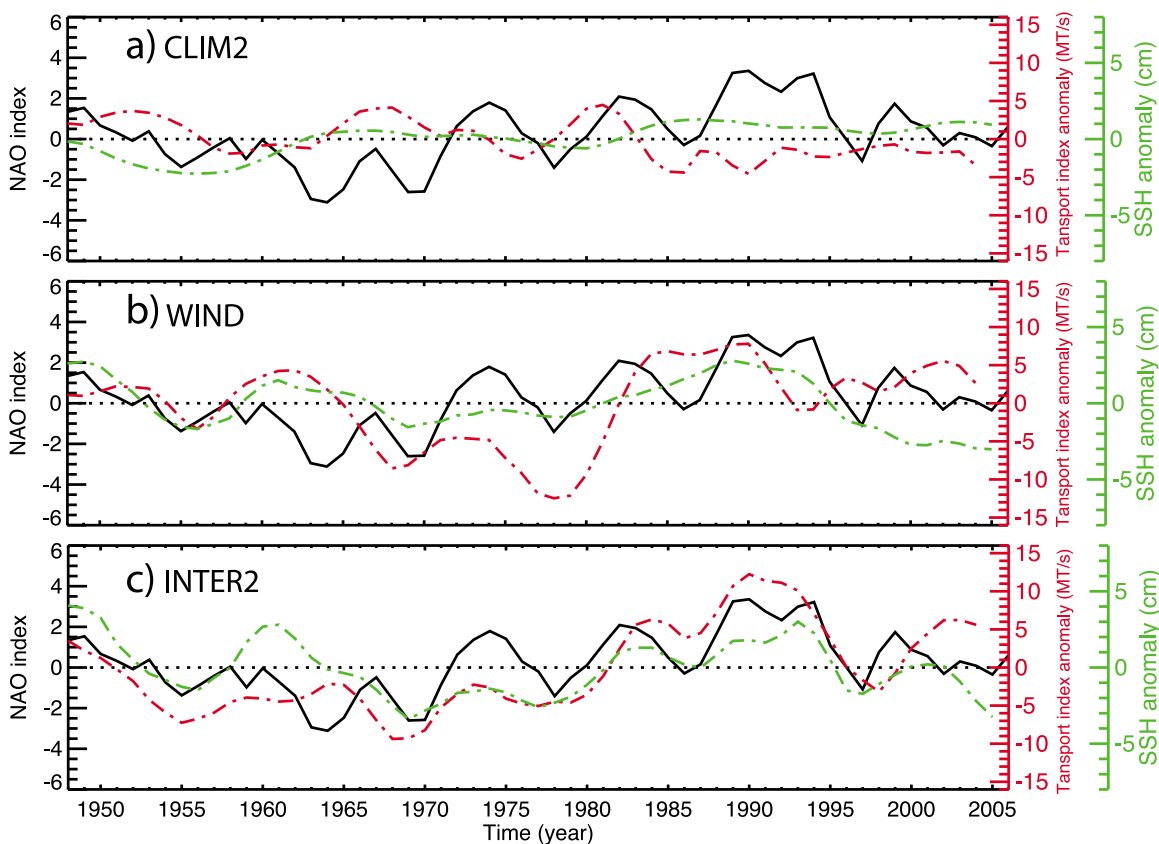


**Figure 13.** Evolution of the NAO index (black), the transport index anomaly (red) between the Labrador Sea and the Bermuda Islands lagged by 2 years and the SSH anomaly (reversed) averaged over the box [60–15°W, 50–65°N] (green) lagged by 1 year, for (a) CLIM2, (b) WIND and (c) INTER2. The subtracted mean is the mean for the period 1948–2006.

box 3 are no longer significantly anti-correlated. We suggest that the lack of correlation between the salinity in box 1 and in the Rockall Trough after 1999 might be explained by the fact that NAO is in a “weak” intermediate phase during this period (see Figure 9d), in contrast to the 1950–1970 period (strong negative phase) and the 1975–1995 period (strong positive phase). Moreover, using numerical experiments, *Hätun et al.* [2005] showed that salinity changes in the Rockall Trough after 1995 resulted from a change of the subpolar gyre circulation, more specifically of the location and strength of the North Atlantic Current. Later, *Lohmann et al.* [2009], also using numerical models, showed a decrease of the subpolar gyre strength after an extended period (10-year) of positive NAO forcing; this weakening was mostly caused by an advection of warm water from the subtropics. These results suggest that dynamics other than those associated with NAO were dominant during this time period in the Rockall Trough. As such, further investigation into the evolution of the Rockall Trough salinity field in our experiment is needed for this particular time period.

## 6. Discussion

[49] We have shown that MOW variability in the Atlantic Ocean during the last 60 years depends on the varying northward and westward transports in the eastern North Atlantic and on variable water mass formation. To evaluate how well our

model reproduces the water mass transport in the North Atlantic, in particular at depth, we show, in Figure 13, the baroclinic mass transport index (0–2000 db) deduced from the anomaly of Potential Energy Anomaly (PEA) between the Labrador Sea and the Bermuda Islands that *Curry and McCartney* [2001] calculated from observations. This transport index represents the eastward transport between the subpolar gyre and the subtropical gyre. We compare the INTER2 transport index with the NAO index and the INTER2 SSH anomaly averaged over the subpolar gyre [60–15°W, 50–65°N] (Figure 13c). We find a significant correlation between the INTER2 transport index and the NAO maximum with a 2-year lag ( $r = 0.71$ ;  $p < 0.01$ ) in agreement with the observations [*Curry and McCartney*, 2001]. We also find a lower but still significant correlation ( $r = 0.33$ ;  $p < 0.01$ ) with a 2-year lag for WIND (Figure 13b). The transport index averaged over 1950–2000 found by *Curry and McCartney* [2001] is 60 MT/s (megatons per second), and is calculated at 65.9 MT/s in the GDEM3 climatology. The same calculation gives 66.8 MT/s in INTER2, 74.5 MT/s in WIND and 74.3 MT/s in CLIM2. Thus, we conclude that the large scale circulation of the North Atlantic, as represented by this transport index is adequately represented in INTER2. Finally, we note that the high transport index for WIND is attributed to the constant buoyancy forcing applied throughout its simulation. This buoyancy forcing was extracted from ERA15, which is a climatology based on the high NAO period 1979–

1993. Thus, LSW formation is constantly on the high side, enhancing the circulation between the two gyres.

## 7. Conclusions

[50] Possible sources of MOW variability include a change in the Mediterranean Sea Water, a change in the North Atlantic Central Water, or a change of the North Atlantic circulation resulting in a shift of the preferred MOW pathway. In an observational analysis, *Lozier and Sindlinger* [2009] showed that the variability of MSW and NACW is too weak to explain the observed MOW variability. In this study, we investigated the third possible source of MOW variability in the Atlantic Ocean using the Hybrid Coordinate Ocean Model (HYCOM).

[51] The first part of this study tested the viability of this hypothesis with a set of model runs. Configured for the North Atlantic and combined with the Marginal Sea Boundary Condition model (MSBC), two 59-year simulations, forced by either a climatological forcing (steady state simulation, CLIM1) or an interannual atmospheric forcing (1948–2006 period, INTER1) were performed. The observed trends in the MOW reservoir were reproduced in the interannual simulation, demonstrating that MOW reservoir variability can be explained by variable atmospheric forcing that induces changes in the circulation of the North Atlantic.

[52] In the second part of this study, three simulations of 59 years (1948–2006) were performed using a 1/3° North Atlantic configuration of HYCOM: one forced with climatological wind stress and buoyancy forcing, the second forced with interannual wind stress and climatological buoyancy forcing, and the third forced with interannual wind stress and buoyancy forcing. Only the simulation using interannual buoyancy and wind stress forcing was able to reproduce the observed trends in temperature and salinity of the MOW reservoir. The comparison of the mid-depth salinity between 1955 and 1970 and 1980 and 1995 shows a negative salinity anomaly north of the reservoir and a positive anomaly west of the reservoir. From an analysis of the MOW transports out of the reservoir we were able to show that the cause of these property changes is a shift of the MOW dominant pathway from northward during 1955–1970 to westward 1980–1995. While WIND presents a significant anti-correlation between the northward and westward transport as in INTER2, our analysis shows that buoyancy forcing is necessary to reproduce the observed property fields. As a consequence of the pathway shifts, salinity anomalies along the northern pathway, specifically in the Rockall Trough, are out of phase with salinity anomalies along the westward pathway in the subtropical gyre. Thus, our work has shown that the observed salinity changes in the MOW reservoir can be explained solely by circulation-induced shifts in the salinity field in the eastern North Atlantic basin. Furthermore, though this study does not explicitly rule out the possibility that NACW and/or MSW change has impacted MOW reservoir property changes, past studies have done so. We conclude, therefore, that circulation changes are the only viable mechanism to explain the observed MOW reservoir changes over the time period studied.

## Appendix A: Implementation of the MSBC Model in HYCOM

[53] The first step in implementing the Price–Yang MSBC model is to define the Gulf of Cadiz boundary zone at the

initialization stage of each model run. The meridional boundary of this zone must be located sufficiently far to the west of the Strait of Gibraltar so that water depths exceed 1500 m to permit the unimpeded injection of overflow water. The meridional boundary is therefore chosen as the first column of grid points west of the Strait where a maximum depth of 1500 m is encountered at two or more grid points within this column. This column is defined by index  $i_1$ . All grid points in and to the east of this column within the Gulf of Cadiz are then considered to be part of the boundary zone. The latitude range over which water is exchanged between the interior Atlantic and the boundary zone consists of all grid points in this column beginning with the first point located south of the latitude of the Strait and extending northward to the Iberian coast. These rows are defined by indices  $j_1$  to  $j_2$ . The required input variables for the MSBC model,  $T_{atb}$ ,  $S_{atb}$ ,  $T_{ent}$ , and  $S_{ent}$  (Figure 2) are obtained from the first column of grid points to the west of the boundary longitude (index  $i_1 - 1$ ). The MSBC model always sets current velocity to zero at all  $u$  and  $v$  grid points within the boundary zone. It also initially resets the temperature, salinity, and layer thicknesses at all  $p$  grid points within the boundary zone to their climatological values, with the exception of the model layers that receive the injected MOW.

[54] The primary difficulty associated with injecting Mediterranean overflow water is that this water must be accepted by interior isopycnic layers with discrete target densities that do not match the density of the overflow water. The simplest way to do this would be to identify the model layer located just west of the boundary zone that spanned the MOW injection depth calculated by the MSBC model, inject the MOW transport calculated by MSBC into this layer with the temperature and salinity values calculated by the MSBC model, and then rely on the hybrid vertical coordinate grid generator to re-establish isopycnic conditions in the layer. However, this requires the grid generator to move model interfaces large distances during each time step, which induces large numerical diffusivity and produces highly uneven layer thicknesses in the MOW tongue west of the Gulf of Cadiz. It was therefore necessary to inject the water in a manner that preserved the isopycnic target densities in the receiving layers.

[55] The first step of this procedure is to identify the two isopycnic layers with target potential densities that bracket the MOW density calculated by the HYCOM equation of state:

$$\sigma_{out} = \sigma(T_{out}, S_{out}, p_0),$$

where  $p_0$  is the reference pressure and potential density is calculated in sigma units.

[56] All overflow water is accepted by these layers, denoted by indices  $k_1$  and  $k_2$ , and separated by interfaces located at pressure depths  $p_{k1}$ ,  $p_{k2}$ , and  $p_{k3}$  (Figure A1). The procedure to partition the MOW injection into the two layers is designed to ensure, to the greatest extent possible, that the mass-weighted average temperature of the injected water equals  $T_{out}$  calculated by the MSBC model. Within the boundary zone, the salinity in the two selected layers is set to  $S_{out}$  calculated by the MSBC model, and then the temperature in each layer is set to

$$T_{k1out} = \sigma^{-1}(\sigma_{k1}, S_{out}, p_0),$$

$$T_{k2out} = \sigma^{-1}(\sigma_{k2}, S_{out}, p_0)$$

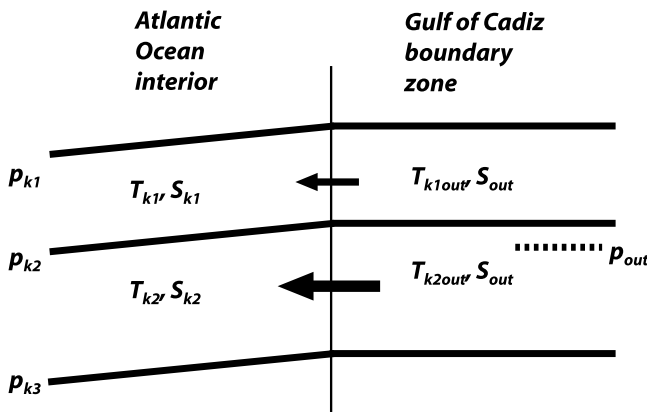


**Figure A1.** Schematic diagram illustrating the two layers chosen to accept the MOW injected from (right) the Gulf of Cadiz boundary zone into (left) the interior North Atlantic. The solid arrows illustrate the partition of the MOW transport between the two layers while the dashed line shows the central pressure depth of the injected water calculated by the MSBC model.

where  $\sigma^{-1}$  signifies the inversion of the equation of state built into HYCOM to calculate temperature from potential density and salinity, and where  $\sigma_{k1}$  and  $\sigma_{k2}$  are the isopycnic target potential densities of the two layers. The pressure depth of the intermediate interface  $p_{k2}$  within the boundary zone is then reset to

$$\hat{p}_{k2} = \begin{cases} p_{out} + (0.5 - q)(p_{k2} - p_{k1}) & q \leq 0.5 \\ p_{out} + (0.5 - q)(p_{k3} - p_{k2}) & q > 0.5 \end{cases},$$

where

$$q = \frac{T_{k1out} - T_{out}}{T_{k1out} - T_{k2out}},$$

and where  $p_{out}$  is the central pressure depth of the injected overflow water. Note that  $q$  must be bounded between 0 and 1 because these limits can be exceeded due to the nonlinear equation of state since the two layers were selected based on their target potential densities and not temperature. The interface pressure depths above and below the two layers are then given by

$$\hat{p}_{k1} = \hat{p}_{k2} + p_{k1} - p_{k2}$$

$$\hat{p}_{k3} = \hat{p}_{k2} + p_{k3} - p_{k2}$$

[57] All other interfaces above and below these three within the boundary zone are set to their climatological mean pressure depths, except to maintain a minimum thickness of 5 m.

[58] With layer thicknesses and water properties set at all of the grid points within the boundary zone, MOW injection into the interior Atlantic is accomplished by partitioning the total zonal transport  $U_{out}$  provided by the MSBC model among the two accepting layers as

$$Tr_{k1} = (1 - q)Tr_{out}$$

$$Tr_{k2} = qTr_{out}$$

[59] It is implemented by controlling the zonal velocity at the column of  $u$  grid points located immediately west of column  $i_1$  of the pressure grid points that represent the off-shore edge of the boundary zone. The zonal transport of the injected water in each layer is distributed over both the layer thickness and the meridional distance between grid point rows  $j_1$  and  $j_2$ . To ensure that there is no net zonal transport between the interior Atlantic and the boundary zone, the other two zonal transports at the edge of the boundary zone calculated by the MSBC model ( $Tr_{atl}$  and  $Tr_{ent}$ ) must also be accounted for. Both of these transports are distributed over the same latitude range (from  $j_1$  to  $j_2$ ) as  $Tr_{out}$ , but  $Tr_{atl}$  is distributed over the upper 140 m while  $Tr_{ent}$  is distributed over the depth range between 140 m and  $p_{k1}$ .

[60] **Acknowledgments.** The authors thank Zulema Garraffo for her help in this work and Kristi Cashman-Burkholder for providing the HYDROBASE/ODV. This research was supported by the National Science Foundation. Simulations were performed at the National Center of Atmospheric Research (NCAR), Boulder, Colorado.

## References

- Artale, V., S. Calmanti, P. Malanotte-Rizzoli, G. Pisacane, V. Rupolo, and M. Tsimplis (2006), The Atlantic and Mediterranean Sea as connected systems, in *Mediterranean Climate Variability*, edited by P. Lionello, P. Malanotte-Rizzoli, and R. Boscolo, pp. 283–322, Elsevier, Oxford, U. K.
- Baringer, M. O., and J. Price (1997), Mixing and spreading of the Mediterranean outflow, *J. Phys. Oceanogr.*, *27*, 1654–1677, doi:10.1175/1520-0485(1997)027<1654:MASOTM>2.0.CO;2.
- Béthoux, J. P., and B. Gentili (1999), Fonctionning of the Mediterranean Sea: Past and present changes related to freshwater input and climatic changes, *J. Mar. Syst.*, *20*, 33–47, doi:10.1016/S0924-7963(98)00069-4.
- Bleck, R. (2002), An oceanic general circulation model framed in hybrid isopycnic-Cartesian coordinates, *Ocean Modell.*, *4*, 55–88, doi:10.1016/S1463-5003(01)00012-9.
- Bower, A. S., B. Lecann, T. Rossby, W. Zenk, J. Gould, K. Speer, P. L. Richardson, M. D. Prater, and H.-M. Zhang (2002), Directly measured mid-depth circulation in the northeastern North Atlantic Ocean, *Nature*, *419*, 603–607, doi:10.1038/nature01078.
- Chassignet, E. P., L. T. Smith, G. T. Halliwell, and R. Bleck (2003), North Atlantic simulations with the Hybrid Coordinate Ocean Model (HYCOM): Impact of the vertical coordinate choice, reference pressure, and thermohalinity, *J. Phys. Oceanogr.*, *33*, 2504–2526, doi:10.1175/1520-0485(2003)033<2504:NASWTH>2.0.CO;2.
- Curry, R. (2001), HydroBase 2: A Database of Hydrographic Profiles and Tools for Climatological Analysis, 81 pp., technical report, Woods Hole Oceanogr. Inst., Woods Hole, Mass.
- Curry, R., and M. S. McCartney (2001), Ocean gyre circulation changes associated with the North Atlantic Oscillation, *J. Phys. Oceanogr.*, *31*, 3374–3400, doi:10.1175/1520-0485(2001)031<3374:OGCCAW>2.0.CO;2.
- Curry, R. G., M. S. McCartney, and T. M. Joyce (1998), Oceanic transport of subpolar climate signals to mid-depth subtropical waters, *Nature*, *391*, 575–577, doi:10.1038/35356.
- Garrett, C. (1996), The role of the Strait of Gibraltar in the evolution of the Mediterranean water properties and circulation, in *Dynamic of Mediterranean Straits and Channels*, *CIESM Sci. Ser.*, vol. 2, edited by F. Briand, *Bull. Inst. Oceanogr.*, *17*, 1–19.
- Garrett, C., R. Outerbridge, and K. Thompson (1993), Interannual variability in Mediterranean heat and buoyancy fluxes, *J. Clim.*, *6*, 900–910, doi:10.1175/1520-0442(1993)006<0900:IVIMHA>2.0.CO;2.
- Halliwell, G. R. (2004), Evaluation of vertical coordinate and vertical mixing algorithms in the Hybrid-Coordinate Ocean Model (HYCOM), *Ocean Modell.*, *7*, 285–322, doi:10.1016/j.oceanmod.2003.10.002.
- Hátún, H., A.-B. Sandø, H. Drange, B. Hansen, and H. Valdimarsson (2005), Influence of the Atlantic subpolar gyre on the thermohaline circulation, *Science*, *309*, 1841–1844, doi:10.1126/science.1114777.
- Holliday, N. P. (2003), Air-sea interaction and circulation changes in the northeast Atlantic, *J. Geophys. Res.*, *108*(C8), 3259, doi:10.1029/2002JC001344.
- Holliday, N. P., et al. (2008), Reversal of the 1960s to 1990s freshening trend in the northeast North Atlantic and Nordic Seas, *Geophys. Res. Lett.*, *35*, L03614, doi:10.1029/2007GL032675.
- Hurrell, J. W. (1995), Decadal trends in the North Atlantic Oscillation: Regional temperatures and precipitation, *Science*, *269*, 676–679, doi:10.1126/science.269.5224.676.

- Iorga, M. C., and M. S. Lozier (1999a), Signatures of the Mediterranean outflow from a North Atlantic climatology 1. Salinity and density fields, *J. Geophys. Res.*, *104*, 25,985–26,009, doi:10.1029/1999JC900115.
- Iorga, M. C., and M. S. Lozier (1999b), Signatures of the Mediterranean outflow from a North Atlantic climatology 2. Diagnostic velocity fields, *J. Geophys. Res.*, *104*, 26,011–26,029, doi:10.1029/1999JC900204.
- Large, W. G., J. C. McWilliams, and S. C. Doney (1994), Oceanic vertical mixing: A review and a model with a nonlocal boundary layer parameterization, *Rev. Geophys.*, *32*, 363–403, doi:10.1029/94RG01872.
- Leadbetter, S. J., R. G. Williams, E. L. McDonagh, and B. A. King (2007), A twenty year reversal in water mass trends in the subtropical North Atlantic, *Geophys. Res. Lett.*, *34*, L12608, doi:10.1029/2007GL029957.
- Levitus, S., J. I. Antonov, T. P. Boyer, and C. Stephens (2000), Warming of the world ocean, *Science*, *287*, 2225–2229, doi:10.1126/science.287.5461.2225.
- Lohmann, K., H. Drange, and M. Bentsen (2009), Response of the North Atlantic subpolar gyre to persistent North Atlantic Oscillation like forcing, *Clim. Dyn.*, *32*, 273–285, doi:10.1007/s00382-008-0467-6.
- Lozier, M. S., and L. Sindlinger (2009), On the source of Mediterranean Overflow Water property changes, *J. Phys. Oceanogr.*, *39*, 1800–1817, doi:10.1175/2009JPO4109.1.
- Lozier, M. S., and N. M. Stewart (2008), On the temporally varying penetration of Mediterranean overflow waters and eastward penetration of Labrador Sea Water, *J. Phys. Oceanogr.*, *38*, 2097–2103, doi:10.1175/2008JPO3908.1.
- Lozier, M. S., W. B. Owens, and R. G. Curry (1995), The climatology of the North Atlantic, *Prog. Oceanogr.*, *36*, 1–44, doi:10.1016/0079-6611(95)00013-5.
- Mazé, J. P., M. Arhan, and H. Mercier (1997), Volume budget of the eastern boundary layer off the Iberian Peninsula, *Deep Sea Res., Part I*, *44*, 1543–1574, doi:10.1016/S0967-0637(97)00038-1.
- McCartney, M., and C. Mauritzen (2001), On the origin of the warm inflow to the Nordic Seas, *Prog. Oceanogr.*, *51*, 125–214, doi:10.1016/S0079-6611(01)00084-2.
- National Geophysical Data Center (1985), Worldwide gridded bathymetry DBDB5 5-min latitude/longitude grid, *Data Announce. 85-MGG-01*, 75 pp., NOAA Natl. Geophys. Data Cent., Boulder, Colo.
- New, A. L., S. Barnard, P. Herrmann, and J.-M. Molines (2001), On the origin and pathway of saline inflow to the Nordic Seas: Insights from the models, *Prog. Oceanogr.*, *48*, 255–287, doi:10.1016/S0079-6611(01)00007-6.
- Pinardi, N., and E. Masetti (2000), Variability of the large scale general circulation of the Mediterranean Sea from observations and modelling: A review, *Palaeogeogr. Palaeoclimatol. Palaeoecol.*, *158*, 153–173, doi:10.1016/S0031-0182(00)00048-1.
- Potter, R. A., and M. S. Lozier (2004), On the warming and salinification of the Mediterranean outflow waters in the North Atlantic, *Geophys. Res. Lett.*, *31*, L01202, doi:10.1029/2003GL018161.
- Price, J. F., and M. O. Baringer (1994), Outflows and deep water production by marginal seas, *Prog. Oceanogr.*, *33*, 161–200, doi:10.1016/0079-6611(94)90027-2.
- Price, J. F., and J. Yang (1998), Marginal sea overflows for climate simulations, in *Ocean Modeling and Parameterization*, edited by E. P. Chassignet and J. Verron, pp. 155–170, Kluwer Acad., Washington, D. C.
- Reid, J. L. (1979), On the contribution of the Mediterranean Sea outflow to the Norwegian-Greenland Sea, *Deep Sea Res., Part A*, *26*, 1199–1223, doi:10.1016/0198-0149(79)90064-5.
- Reid, J. L. (1994), On the total geostrophic circulation of the North Atlantic Ocean: Flow patterns, tracers, and transports, *Prog. Oceanogr.*, *33*, 1–92, doi:10.1016/0079-6611(94)90014-0.
- Teague, W. J., M. J. Carron, and P. J. Hogan (1990), A comparison between the Generalized Digital Environmental Model and Levitus climatologies, *J. Geophys. Res.*, *95*, 7167–7183, doi:10.1029/JC095iC05p07167.
- Xu, X., E. P. Chassignet, J. F. Price, T. M. Özgökmen, and H. Peters (2007), A regional modeling study of the entraining Mediterranean outflow, *J. Geophys. Res.*, *112*, C12005, doi:10.1029/2007JC004145.
- Zenk, W. (1975), On the Mediterranean outflow west of Gibraltar, *Meteor. Forschungsber.*, *Reihe A*, *16*, 23–24.

A. Bozec and E. P. Chassignet, Center for Ocean and Atmospheric Predictions Studies, Florida State University, 227 RM Johnson Bldg., 2035 E. Paul Dirac Dr., Tallahassee, FL 32310, USA. (abozec@coaps.fsu.edu)

G. R. Halliwell, Atlantic Oceanographic and Meteorological Laboratory, NOAA, 4301 Rickenbacker Cswy., Miami, FL 33149, USA.

M. S. Lozier, Earth and Ocean Sciences, Nicholas School of the Environment, Duke University, Box 90227, Durham, NC 27708, USA.